Acta Pharmaceutica Sinica B 2025;15(6):3073−3091

Chinese Pharmaceutical Association
Institute of Materia Medica, Chinese Academy of Medical Sciences

Acta Pharmaceutica Sinica B

www.elsevier.com/locate/apsb
www.sciencedirect.com

ORIGINAL ARTICLE

An anti-complement homogeneous polysaccharide from *Houttuynia cordata* ameliorates acute pneumonia with H1N1 and MRSA coinfection through rectifying Treg/Th17 imbalance in the gut−lung axis and NLRP3 inflammasome activation

Xinxing Li[a,†], Wenxin Ding[b,†], Yan Lu[a], Haiyan Zhu[b], Weilian Bao[a], Yang Liu[a], Jiaren Lyu[a], Lishuang Zhou[a], Hong Li[c,*], Jiyang Li[b,*], Daofeng Chen[a,*]

[a]*Department of Natural Medicine, School of Pharmacy, Fudan University, Shanghai 201203, China*
[b]*Department of Biological Medicines, School of Pharmacy, Fudan University, Shanghai 201203, China*
[c]*Department of Pharmacology, School of Pharmacy, Fudan University, Shanghai 201203, China*

Received 11 October 2024; received in revised form 16 January 2025; accepted 27 January 2025

KEY WORDS

Houttuynia cordata;
Polysaccharides;
H1N1;
MRSA;
Pneumonia;
Complement;
NLRP3;
Treg/Th17 cell balance;
Gut-lung axis

Abstract The coinfection of respiratory viruses and bacteria is a major cause of morbidity and mortality worldwide, despite the development of vaccines and powerful antibiotics. As a macromolecule that is difficult to absorb in the gastrointestinal tract, a homogeneous polysaccharide from *Houttuynia cordata* (HCPM) has been reported to exhibit anti-complement properties and alleviate influenza A virus (H1N1)-induced lung injury; however, the effects of HCPM without *in vitro* antiviral and antibacterial activities on more complicated pulmonary diseases resulting from viral-bacterial coinfection remains unclear. This study established a representative coinfection murine pneumonia model infected with H1N1 (0.2 LD_{50}) and methicillin-resistant *Staphylococcus aureus* (MRSA, 10^7 CFU). HCPM significantly improved survival rate and weight loss, and ameliorated gut−lung damage and inflammatory cytokine production. Interestingly, the therapeutic effect of HCPM on intestinal damage preceded that in the lungs.

---

*Corresponding authors.

E-mail addresses: dfchen@shmu.edu.cn (Daofeng Chen), lijiyang@fudan.edu.cn (Jiyang Li), lxzhang@shmu.edu.cn (Hong Li).

[†]These authors made equal contributions to this work.

Peer review under the responsibility of Chinese Pharmaceutical Association and Institute of Materia Medica, Chinese Academy of Medical Sciences.

https://doi.org/10.1016/j.apsb.2025.04.008

Mechanistically, HCPM inhibited the overactivation of the intestinal complement (C3a and C5a) and suppressed the activation of the NLR family pyrin domain-containing 3 (NLRP3) pathway, which contributes to the regulation of the Treg/Th17 cell balance in the gut—lung axis. The results indicate the beneficial effects of an anti-complement polysaccharide against viral—bacterial coinfection pneumonia by modulating crosstalk between multiple immune regulatory networks.

1. Introduction

Pulmonary infections caused by viral and bacterial coinfection are serious diseases threatening human life. Studies have shown that coronavirus disease 2019 (COVID-19) patients with a bacterial coinfection or secondary infection have a higher in-hospital mortality and longer length of hospitalization[1,2]. Most influenza-related deaths occur from bacterial superinfections rather than the direct effects of the influenza virus[3]. During other respiratory viral infections, such as the Middle East respiratory syndrome and severe acute respiratory syndrome, the incidence of bacterial coinfection was reported as 1%—19%[4-6] and 1%—43%[4], respectively. Of note, methicillin-resistant *Staphylococcus aureus* (MRSA) is the most commonly encountered coinfections bacterium associated with multiple respiratory infections including the influenza pandemic and COVID-19. Currently, the clinical treatment for virus—bacterium coinfection pneumonia includes a combination of antiviral drugs and antibiotics. Coinfection of viruses and bacteria can quickly develop into severe, necrotizing pneumonia, causing over 50% mortality despite antibiotic treatment[7]. Antibiotics or antiviral drugs work directly against the pathogen. Respiratory coinfections involve complex interactions between viruses/bacteria and the host[8,9]. Therefore, targeting the host immune system might be the potential strategy for coinfection treatment without the risk of antiviral and/or antibiotic resistance[8].

The complement system is an important component of the innate immune system and is vital for the host defense against microbial infections[10,11]. However, the inappropriate activation of the complement system is involved in the pathogenesis of multiple tissue injuries and acute inflammatory diseases, such as acute respiratory distress syndrome[12-14]. The complement activation products, anaphylatoxins C3a and C5a, activate the inflammatory response as well as fatal shock-like syndrome[12,15]. Anti-C5a antibody or anti-C3 agents (such as AMY-101) can lead to immediate clinical improvement in COVID-19[16]. Regulation of complement activity may be beneficial for the treatment of a wide range of complement-associated diseases[16,17].

C3a and C5a induce the NLR family pyrin domain-containing 3 (NLRP3) inflammasome[18-21]. Activated NLRP3 binds to its adaptor, apoptosis-associated speck-like protein containing a CARD (ASC), which in turn, interacts with caspase-1 to form a complex known as the inflammasome, leading to caspase-1 activation. Caspase-1 subsequently cleaves the proinflammatory cytokines IL-1β and IL-18 into their active forms, thus contributing to an uncontrolled inflammatory response[22,23]. Many studies have shown that the NLRP3 inflammasome is an important molecular pathway that mediates the response against a myriad of pathogenic microbial infections[24]. However, NLRP3 appears to play a different role in mice during viral and bacterial pneumonia[24]. In NLRP3$^{-/-}$ mice, the survival rate during viral infection is decreased[24]. Bacterial infection of mice lacking NLRP3 results in decreased lung inflammation, which indicates its protective role[25].

An imbalance between Treg and Th17 cells has been observed in the majority of pulmonary inflammatory diseases[26-28]. More importantly, our previous study has shown that the migration of Treg/Th17 cells in the gut-lung axis is affected by the chemokine CCR6 and its ligand CCL20, and confirmed that Treg/Th17 cells in the gut-associated lymphoid tissue (GALT) affect Treg/Th17 cells in the lung mucosa through CCR6—CCL20 axis[26]. Interestingly, multiple lines of evidence suggest that the NLRP3 inflammasome is involved in Treg/Th17 cell balance in multiple models of inflammation, including asthma[23], arthritis[29], and ulcerative colitis[30]. Nevertheless, the effects of complement, the NLRP3 inflammasome, and Treg/Th17 cells in the viral—bacterial coinfection murine model remain uncertain.

As a traditional Chinese medicine (TCM) that clears heat and eliminates toxins, the *Houttuynia cordata* Thunb. is commonly used for the treatment of infectious lung diseases, cancer, and anaphylaxis[31-33]. Polysaccharides from *Houttuynia cordata*, as macromolecular substances that are not easily absorbed into the blood, have attracted much attention because of their prominent immunomodulatory effects[26]. In our previous studies, crude polysaccharides from *Houttuynia cordata* (HCP) and/or a homogeneous polysaccharide from *Houttuynia cordata* (HCPM) ameliorated lung injury induced by influenza A virus (H1N1) or lipopolysaccharide. The primary mechanism was associated with the inhibition of the excessive activation of the complement system and inflammation[11,34,35]. The results indicated that anti-complementary polysaccharide may be a key active substance in HCP for treating pulmonary infection.

Crosstalk between the gut and lung, known as the “gut—lung axis”, is critical for the immune response in respiratory diseases[36]. Interestingly, the intestine has often been viewed as a potential target organ for polysaccharides[37,38]. Our previous studies indicate that HCP has significant anti-complement properties that alleviate H1N1-induced pneumonia by regulating the Treg/Th17 cell balance in the gut—lung axis[26]. However, whether this anti-complementary polysaccharide can modulate the complement system and T cell homeostasis and thus exert a beneficial effect in a virus and bacteria coinfection model, especially drug-resistant bacteria including MRSA, remains unclear. The specific mechanism of action of this polysaccharide is also unknown.

In this study, we used the H1N1—MRSA coinfection mouse model to examine the therapeutic effects and potential immunomodulatory mechanisms of HCPM on virus-bacterium coinfection-induced severe pneumonia. We evaluated the multi-target effects of HCPM in this coinfection model in terms of complement, NLRP3 inflammasome, and Treg/Th17 cell balance.

2. Materials and methods

2.1. *Reagents and antibodies*

PBS (#ST476), RIPA lysis buffer (#P0013B), phenylmethanesulfonyl fluoride solution (PMSF, #ST507), SDS-PAGE gel preparation kit (#P0012A), TBS with tween-20 (TBST, #ST673), Na, K-ATPase $\alpha1$ rabbit monoclonal antibody (#AG1183), GAPDH rabbit monoclonal antibody (#AF1186), and HRP-labeled goat anti-rabbit IgG (H + L) (#A0208) were purchased from Beyotime (Shanghai, China). Xylene (#10023418) and absolute ethanol (#100092680) were obtained from Sinopharm Chemical Reagent Co., Ltd. (Shanghai, China). Isoflurane (#20220801) was obtained from Jindafu Pharmaceutical Co., Ltd. (China). Mannitol salt agar (#HB4128) and nutrient broth (NB, #HB0108) were purchased from Qingdao Hope Biotechnology Company (China). Nonfat dry milk (#1706404) was purchased from Bio-Rad (Hercules, CA, USA). MCC950 (#M8083) was obtained from AbMole BioScience (Houston, TX, USA). ZO-1 (#21773-1-AP) antibody was purchased from Proteintech (Rosemont, IL, USA). Claudin-1 (#sc-166338) and Occludin (#sc-133256) were obtained from Santa Cruz Biotechnology (Dallas, TX, USA). NLRP3 (#T55651), Cleaved-caspase-1 (#TA4022), and Caspase-1 (#PA5426) were purchased from Abmart (Shanghai, China). ASC (#13833S) antibody was purchased from Cell Signaling Technologies (Beverly, MA, USA). Complement C3a (#144-60264) antibody was obtained from RayBiotech (Atlanta, GA, USA). Complement C5a (#PA5-78891) antibody was purchased from Thermo Fisher Scientific (Waltham, MA, USA). H1N1 NP (#NB100-56570) was purchased from Novus Biologicals (Littleton, CO, USA). The ELISA kits for mouse TNF-α (#EK282/4-96), mouse IL-6 (#EK206/3-96), mouse MPO (#EK2133/2-96), mouse IFN-γ (#EK280/3-96), mouse IL-10 (#EK210/4-96), mouse IL-17A (#EK217/2-96), mouse IL-18 (#EK218), and mouse IL-1β (#EK201B) were purchased from Multisciences Biotech Company (Hangzhou, China). Mouse IFN-α (#EMC035a) and mouse IFN-β (#EMC016) were purchased from Neobioscience (Shenzhen, China).

2.2. *Animals, virus, and bacterial strain*

Female mice were firstly selected to establish the H1N1 and MRSA coinfection model according to our previous experience in a mouse model of H1N1 infection. C57BL/6 female mice (14−16 g, four weeks old) were purchased from Slaccas Experimental Animal Inc. (Shanghai, China). The mice were housed in a specific-pathogen-free environment with a controlled temperature of 24 ± 2 °C and subjected to a 12-h light/dark cycle with free access to food and water. The animal experiments were approved by the Animal Ethics Committee of Fudan University (License number: 2020-09-SY-LJY-01) and carried out in compliance with the guidelines.

The mouse-adapted influenza A virus strain (A/FM/1/47, H1N1) was provided by Dr. Haiyan Zhu (School of Pharmacy, Fudan University). The half-lethal dose (LD_{50}) for H1N1 virulence was calculated by the method of Reed-Muench[39]. The virus was re-packaged and stored at −80 °C. MRSA-20-385 (Ethical number: 2019-460) was obtained from the Huashan Hospital Affiliated to Fudan University (Shanghai, China). The bacterial strains were stored at −80 °C in brain heart infusion broth supplemented with 20% glycerol. The bacteria were inoculated in 6 mL of nutrient broth (#HB0108, Qingdao Hope Bio-Technology Company) at a ratio of 1:100 and shaken horizontally at 180 rpm for 18 h at 37 °C in a constant temperature shaker (Jing Hong Laboratory Instrument Company, Shanghai, China). After two growth cycles, turbidity was calculated using a turbidity meter (#WZT-1M, Jinjia Scientific Instrument Company, Shanghai, China). The bacterial pellets were collected following centrifugation. The pellets were washed twice with sterile sodium chloride solution (#L222062507, Sichuan Kelun Pharmaceutical Company, Chengdu, China) and diluted to three experimental concentrations of 10^8, 10^7, and 10^6 colony-forming units (CFU) based on the turbidity [40].

2.3. *Cellular toxicity of Houttuynia cordata polysaccharides on Madin−Darby canine kidney (MDCK) cells*

Cellular toxicity was measured as described previously with minor modification[41]. Briefly, MDCK cells were seeded into 96-well plates (5×10^4 cells/well) and cultured for 14 h. The cells were then treated with HCPM (50, 100, and 200 μg/mL) or HCP (200 μg/mL) for 24 h. Toxicity was determined using an MTT assay kit (#C0009S, Beyotime, Shanghai, China) based on the manufacturer's instructions. The absorbance was measured with a microplate reader (Thermo Scientific, Waltham, MA, USA) at 570 nm.

2.4. *In vitro anti-influenza virus H1N1 effect*

An *in vitro* anti-H1N1 assay was conducted as described previously[42]. MDCK cells were seeded into 96-well plates (5×10^4 cells/well) overnight and infected with the H1N1 virus (2×10^{-4}) for 2 h. The cells were then treated with HCPM (50, 100, and 200 μg/mL) or HCP (200 μg/mL) for 3 days. A cytopathic effect reduction assay was used to evaluate the antiviral effects of the test samples.

2.5. *In vitro anti-MRSA assay*

An *in vitro* anti-MRSA assay was performed as described previously[43]. Briefly, bacterial suspensions were added to a nutrient broth at a final concentration of 10^6 CFU/mL. The bacterial suspensions were treated with HCPM or HCP for 24 h. Finally, the OD_{600nm} of each well was measured using a microplate reader to determine the concentration that inhibited MRSA growth.

2.6. *Murine model of viral-bacterial coinfection*

To construct a milder coinfection model consistent with the characteristics of TCM, we further explored the infective dose of MRSA based on 0.2 LD_{50} H1N1[44]. C57BL/6 mice were infected intranasally with an extremely low dose (0.2 LD_{50}) of H1N1, followed by MRSA (10^8, 10^7, or 10^6 CFU) infection three days later during light isoflurane anesthesia. These mice were euthanized on 5/6 days post H1N1 infection (dpi) and the changes in body weight and lung pathology were observed.

2.7. *Treatment with Houttuynia cordata polysaccharides*

The HCPM (Mw, 19.1 kDa) and HCP were prepared and identified by Dr. Lishuang Zhou (School of Pharmacy, Fudan University, Shanghai, China), and relevant chromatograms were reported in the study[35] by Dr. Lishuang Zhou. The dose of HCPM and HCP was based on the results of the previous study[45] and pilot tests. The mouse model in this study was established by coinfection with H1N1 and MRSA. Oseltamivir is a standard antiviral drug for H1N1 influenza virus. Linezolid is an antibiotic used clinically to treat MRSA infections. Although existing study[46] has used Oseltamivir as a positive control for H1N1 and MRSA coinfections, which highlights the importance of antiviral therapy, the status of the bacteria is often neglected. Clinical guidelines[47] suggest the early use of antiviral therapy for influenza patients with bacterial coinfections, followed by the administration of empirical antibiotics depending on the patient's condition. In this study, we designed three positive control groups: Oseltamivir, Linezolid, and Oseltamivir + Linezolid. This is consistent with the clinical guidelines and makes the experimental design more adequate.

Survival experiment: C57BL/6 mice were randomly divided into the following nine groups (11 mice/group): control, H1N1−MRSA coinfection (coinfection), coinfection + HCPM 20 mg/kg, coinfection + HCPM 40 mg/kg, coinfection + HCPM 80 mg/kg, coinfection + HCP 80 mg/kg, coinfection + Oseltamivir 22.75 mg/kg (coinfection + OST), coinfection + Linezolid 200 mg/kg (coinfection + LZD), and coinfection + Oseltamivir (22.75 mg/kg) + Linezolid (200 mg/kg) (coinfection + OST + LZD). Mice in the control group were intranasally administered with 30 μL of sterile sodium chloride solution without H1N1 or MRSA. The other mice were infected intranasally with 0.2 LD_{50} H1N1 (30 μL) and then infected with 10^7 CFU MRSA (30 μL) three days later. The mice in the control group were administered 0.5% sodium carboxymethyl cellulose solution (Aladdin, Shanghai, China) as the vehicle. The other mice were treated with the indicated drugs once daily for seven days *via* gavage, beginning 2 h after viral infection. The survival rate and body weight were continuously monitored for 14 days.

Coinfection-induced pneumonia experiment: All mice were randomly divided into the following nine groups (6 mice/group): control, H1N1−MRSA coinfection (coinfection), coinfection + HCPM 20 mg/kg, coinfection + HCPM 40 mg/kg, coinfection + HCPM 80 mg/kg, coinfection + HCP 80 mg/kg, coinfection + Oseltamivir 22.75 mg/kg (coinfection + OST), coinfection + Linezolid 200 mg/kg (coinfection + LZD), and coinfection + Oseltamivir (22.75 mg/kg) + Linezolid (200 mg/kg) (coinfection + OST + LZD). All drugs were prepared with 0.5% sodium carboxymethyl cellulose solution. The mice were slightly anesthetized using isoflurane and intranasally instilled with 0.2 LD_{50} H1N1 solution. The drugs were orally administered to the relevant infected mice 2 h post-infection once daily starting from Day 0 and continuing to Day 4. The uninfected mice were administered 0.5% sodium carboxymethylcellulose solution as the negative control. The mice were next exposed to 10^7 CFU MRSA intranasally on Day 3. The lungs and small intestines were harvested from the sacrificed mice at 5 dpi for further analysis.

2.8. *Determination of cytokine production by ELISA*

The lung tissues stored at −80 °C were thawed on ice, weighed, and homogenized in a tissue homogenizer with sterile PBS (1:9). The contents of the small intestine were removed with ice PBS before weighing, and subsequent sample treatment was performed as with the lungs. The supernatant was collected after centrifugation at 3000 rpm (#TGL-21M, Bioridge Centrifuge, Shanghai, China) and 4 °C for 10 min to remove any tissue fragments. Cytokine production in the lung samples and small intestinal tissues was measured by ELISA according to the manufacturer's instructions.

2.9. *Assessment of bacterial load*

To detect the bacterial load in mouse lungs, we prepared a mannitol high-salt agar solid culture medium (MRSA selective) in the biosafety cabinet. Next, lung tissues were homogenized with sterile PBS at a ratio of 1:9. Based on a previously reported study[44], the lung homogenate was fivefold gradient diluted and four concentrations (5^0, 5^{-1}, 5^{-2}, and 5^{-3}) were established. Then, 5 μL of each concentration was spotted on the solid culture medium and incubated at 37 °C for 24 h. The total bacterial load in the lungs was calculated.

2.10. *Histological analysis*

To assess pathological damage, the tissues were fixed in 4% paraformaldehyde solution (#BL539A, Biosharp Life Sciences, China) for 48 h and embedded in paraffin. They were sectioned at 5 μm and stained with hematoxylin and eosin (H&E)[48]. The images were captured under an Olympus VS200 slide scanner (Tokyo, Japan) and analyzed using ImageJ software (ImageJ/Fiji 2.1, National Institution of Health, Bethesda, MD, USA). To assess the expression of complement C3a and C5a in the tissues, immunohistochemical staining was performed as described previously[49]. The paraffin tissue sections were incubated successively in citrate antigen retrieval solution (#P0081, Beyotime, Shanghai, China) and endogenous peroxidase blocking buffer (#P0100A, Beyotime, Shanghai, China). The sections were then incubated with anti-C3a antibody (1:100) or anti-C5a antibody (1:100) at 4 °C overnight, followed by HRP-conjugated secondary antibody (1:50) for 60 min. Detection was done using a DAB horseradish peroxidase color development kit (#P0203, Beyotime, Shanghai, China). Image acquisition was done with an inverted phase contrast fluorescence microscope (Olympus, Tokyo, Japan). Positive staining for complement C3a and C5a was analyzed using ImageJ software.

2.11. *Small intestinal mucin staining*

We used a commercial Alcian blue & nuclear fast red staining kit (#C0153S, Beyotime, Shanghai, China) for mucin staining. Small intestine paraffin sections were deparaffinized in xylene for 10 min, followed by rinsing in fresh xylene for an additional 10 min. The sections were then treated with ethanol in descending concentrations (anhydrous, 90%, 80%, and 70%). After staining with Alcian blue and Nuclear Fast Red solutions, sections were rinsed with tap water for 5 min. Slides were dehydrated in graded ethanol solutions and cleared with xylene before mounting with neutral resin. Imaging was done using an inverted phase contrast fluorescence microscope (Olympus, Tokyo, Japan), revealing blue-stained mucin and pink-stained cell nuclei.

2.12. *Western blotting analysis*

Protein detection was performed by Western blotting as described previously[50]. Specifically, lung specimens were lysed using RIPA buffer with 1% PMSF to extract total protein. The protein concentration was determined using a BCA assay kit (#P0010, Beyotime, Shanghai, China). The samples were mixed with 5 × SDS-PAGE loading buffer (#P0286, Beyotime, Shanghai, China), denatured at 95 °C for 10 min, and separated on 10% SDS-PAGE gels. Following electrophoresis, the proteins (20 μg) were transferred to PVDF membranes. The membranes were blocked and then incubated overnight at 4 °C with primary antibodies against Na,K-ATPase $\alpha 1$ (1:1000), H1N1 NP (1:1000), NLRP3 (1:1000), cleaved Caspase-1 (1:1000), Caspase-1 (1:1000), ASC (1:1000), and GAPDH (1:1000). Following incubation with HRP-labeled goat anti-rabbit IgG (H + L) (1:1000) secondary antibody, the signal was detected using the BeyoECL plus detection kit (#P0018S, Beyotime, Shanghai, China) and imaged directly on FluorChem M (ProteinSimple, Silicon Valley, USA).

2.13. *Quantitative real-time PCR*

qRT-PCR analysis was conducted as previously described[51]. Briefly, RNA was extracted using Trizol reagent (#P2141231, Adamas Life, Shanghai, China), followed by cDNA synthesis using a First Strand cDNA Synthesis Kit (#D7182M, Beyotime, Shanghai, China). Real-time qPCR was performed using 2 × SYBR Green qPCR Mix (#D7265, Beyotime, Shanghai, China) on a real-time PCR instrument (Applied Biosystems, Thermo Scientific, Waltham, MA, USA). The influenza A virus M1 (*H1N1 M1*) gene were measured using the following primers: forward primer, 5′-AAGACCAATCCTGTCACCTCTGA-3′; and reverse primer, 5′-CAAAGCGTCTACGCTGCAGTC-3′[44]. Glyceraldehyde-3-phosphate dehydrogenase (*GAPDH*) expression was measured using the following primers: *GAPDH* forward primer, 5′-ACAGCCTCAAGATCATCAGCA-3′; and reverse primer, 5′-ATGAGTCCTTCCACGATACCA-3′[44].

2.14. *Fluorescence microscopy experiments*

Immunofluorescence assays were performed following the instructions of the Multiimmunofluorescence kit (#RC0086-34, Recordbio, Shanghai, China). Paraffin-embedded slides were subject to xylene and ethanol treatment, followed by washing in tap water and PBS. Antigen retrieval was conducted in a citrate solution at 95 °C, and the sections were subsequently blocked and incubated with primary antibodies. After incubation with secondary antibodies and fluorescent dyes, the slides were mounted with an antifade medium containing DAPI (#P0131, Beyotime, Shanghai, China). The slides were visualized under a laser scanning confocal microscope (Olympus, Tokyo, Japan). The positive areas were identified using ImageJ software.

2.15. *Preparation of mouse cells for flow cytometry analysis*

The spleens, Peyer's patches (PPs), and mesenteric lymph nodes (MLNs) were removed from the mice as previously described[52,53]. They were minced and ground with a syringe plug. Tissues and cells were collected and filtered through a sterile 70 μm sieve to remove debris. Red blood cells were lysed using a red blood cell lysis buffer (#420301, BioLegend, San Diego, CA, USA) for 5 min. The obtained cell suspension was washed with sterile PBS and resuspended in RPMI 1640 containing 10% FBS (#C0234, Beyotime, Shanghai, China).

Lung lymphocytes were extracted as previously described[26]. Briefly, lung tissues were minced and digested in prewarmed RPMI 1640 containing 100 U/mL collagenase I (#17100−017, Gibco, Grand Island, NY, USA) and 5% FBS with shaking at 200 rpm for 60 min at 37 °C. The lymphocytes were enriched by 40%/70% cell separation solution (#17089102, Cytiva, Shanghai, China) gradient centrifugation at $1260 \times g$ for 30 min at 4 °C. The cells at the interface were washed with sterile PBS and resuspended in RPMI 1640 containing 10% FBS.

Lamina propria lymphocytes (LPLs) were extracted as previously described[26]. Briefly, LPLs were extracted from dissected small intestine sections lacking PPs and MLNs. The intestinal epithelial cells underwent dissociation in RPMI 1640 solution containing 5 mmol/L EDTA (#C0196, Beyotime, Shanghai, China), 1 mmol/L DTT (#ST041, Beyotime, Shanghai, China), and 5% FBS with agitation at 200 rpm for 20 min at 37 °C. After two rounds of cell dissociation, the remaining segments were minced and digested in RPMI 1640 supplemented with 1 mg/mL collagenase IV (#C5138, Sigma−Aldrich, St. Louis, MO, USA) and 5% FBS, by shaking at 200 rpm for 60 min at 37 °C. Subsequently, the LPLs were enriched by gradient centrifugation of 40%/70% cell separation solution at $1260 \times g$ for 30 min at 4 °C. The collected cells from the interface were washed with sterile PBS and suspended in RPMI 1640 containing 10% FBS.

The frequencies of Treg and Th17 cells in spleens, lung lymphocytes, LPLs, PPs, and MLNs were determined as previously described[26]. Before cell staining, the anti-mouse CD16/32 (#abs9477, Absin, Shanghai, China) antibody was used to block Fc receptors. For Treg cells, surface staining with anti-CD4 antibodies (#11-0041-82, eBioscience, San Diego, CA, USA) was followed by intracellular staining with anti-Foxp3 antibodies (#25-5773-82, eBioscience, San Diego, CA, USA) using the Foxp3/Transcription Factor Staining Buffer kit (#00-5523-00, eBioscience, San Diego, CA, USA). Th17 cells were surface-stained with anti-CD4 antibodies and intracellularly stained with anti-IL-17A antibodies (#25-7177-82, eBioscience, San Diego, CA, USA) using an intracellular fixation and permeabilization kit (#88-8824-00, eBioscience, San Diego, CA, USA). Isotype controls were employed for compensation adjustments. The percentages of Treg and Th17 cells were quantified using the flow cytometer (#CytoFLEX S, Beckman Coulter, Pasadena, CA, USA) with data analysis performed using FlowJo software.

2.16. *Statistical analysis*

Statistical analysis was performed using GraphPad Prism 6.0 software. Group comparisons were conducted using a one-way ANOVA with Dunnett's multiple comparisons test. Data are presented as the mean ± standard deviation (SD), with statistical significance set at $P < 0.05$ ($^{*}P < 0.05$, $^{**}P < 0.01$, $^{***}P < 0.001$).

3. Results

3.1. *HCPM and HCP mitigate pneumonia severity in viral-bacterial coinfection mice*

The severe pneumonia model induced by H1N1−MRSA coinfection was established during the early stage of our laboratory[44]. In this experiment, the H1N1 virus infection dose (0.2 LD_{50}) was kept constant[44], and the MRSA infection dose was reduced at 10^8, 10^7, and 10^6 CFU. Under the same H1N1 infection titer, the high-dose MRSA coinfected group (10^8 CFU) exhibited a significantly increased lung index (about 15) and stronger histopathological damage at 5 dpi (Supporting Information Fig. S1A and S1B). The other two MRSA groups (10^7 and 10^6 CFU) showed similar lung index levels (approx. 12), with only minor surface damage visible in the lungs. However, the lung index for all coinfection groups increased sharply to approximately 19 at 6 dpi (Fig. S1C), with almost the entire lung showing swelling and severe bleeding (Fig. S1A). At this point, the lung index and lung damage response were no longer affected by the MRSA infection dose (Fig. S1A and S1C). The results suggest that secondary MRSA infection after H1N1 infection has a severe impact on the exacerbation of pulmonary inflammatory edema and lung damage during the late stage of infection.

IFN-γ is a typical proinflammatory cytokine that reflects the degree of pulmonary inflammatory damage. Compared with the control group, the high-dose MRSA (10^8 CFU) coinfection group exhibited a significant increase in IFN-γ expression (Fig. S1D and S1E), which was higher than the other two groups treated with lower MRSA doses (10^7 and 10^6 CFU). The results indicate that by keeping the 0.2 LD_{50} H1N1 infection dose unchanged and reducing the MRSA infection dose, secondary infection with 10^7 CFU MRSA results in relatively mild pulmonary inflammation and tissue damage, with small differences within the groups. This indicates that the coinfection model is more stable at this dose. In addition, a previous study[44] has shown that 10^8 CFU mice lose more weight and are prone to death during coinfection, which was difficult for collecting sufficient data in the mechanism study.

Based on the above, 10^7 CFU MRSA was selected to construct the stable coinfection model to explore the efficacy and mechanism of TCM.

Next, we analyzed the differences between H1N1−MRSA coinfection and 0.2 LD_{50} H1N1 or 10^7 CFU MRSA infection. The results indicated that H1N1−MRSA coinfection caused more significant weight loss compared with H1N1 or MRSA infection alone (Fig. S1F). Coinfection caused severe lung damage indicated by the severe disruption of the lung architecture, inflammatory cell infiltration, and alveolar wall thickening (Fig. S1G and S1H). In addition, coinfection markedly increased the virus load (Fig. S1I), MRSA colonization (Fig. S1J), and the proinflammatory cytokines TNF-α (Fig. S1K) and IFN-γ (Fig. S1L) content in the lungs. In addition, coinfection exhibited severe small intestine damage characterized by disheveled and shortened villi, destroyed crypts, and inflammatory cells infiltration (Fig. S1M). In addition, coinfection showed elevated IFN-γ levels in the gut (Fig. S1N).

Treg/Th17 cell imbalance is a key mechanism associated with a variety of inflammatory diseases. Our results indicated that Treg/Th17 cell imbalance in the gut−lung axis was much more severe in the H1N1−MRSA coinfection group compared with that in the H1N1 or MRSA group (Supporting Information Fig. S2). Therefore, coinfection of H1N1 (0.2 LD_{50}) and MRSA (10^7 CFU) at extremely low doses leads to severe lung-gut injury, which to some extent reflects the lung-gut symptoms observed in influenza patients with coinfections.

To establish a stable and feasible coinfection model that is better adapted to ethical requirements, mice were infected with 10^7 CFU MRSA three days following 0.2 LD_{50} H1N1 infection. The potential efficacy of *Houttuynia cordata* polysaccharides was examined in the coinfection model.

The *in vitro* results indicated that both HCPM and HCP had no *in vitro* anti-H1N1 (Supporting Information Fig. S3) and anti-MRSA (Supporting Information Fig. S4) activities. The 14-day survival results indicated that coinfection mice died from 7 days post virus infection (Fig. 1A). The survival rates in the HCPM (80 mg/kg) and HCP (80 mg/kg) groups were 36% and 10%, respectively. In terms of weight change (Fig. 1B), the body weight of all infected mice decreased after 4 dpi. The HCPM (80 mg/kg) and HCP (80 mg/kg) treatment groups showed a tendency to gain weight after 12 dpi. Collectively, our results suggest that HCPM and HCP can improve the survival rate and body weight of coinfection mice.

As shown in Fig. 1C, HCPM, HCP, Oseltamivir, or Oseltamivir + Linezolid combination treatment decreased the lung index, whereas Linezolid treatment did not show an obvious effect. Coinfection induced remarkable histopathological lesions in the lungs, which was evident by severe disruption of the normal lung architecture, inflammatory cell infiltration, and alveolar wall thickening, all of which were alleviated in the HCPM group, HCP group, Oseltamivir group, and Oseltamivir + Linezolid combination group (Fig. 1D). Damage to Na,K-ATPase $\alpha1$ activity expression destroys alveolar fluid clearance[54]. The results indicated that HCPM and HCP significantly enhance the Na,K-ATPase $\alpha1$ activity (Fig. 1E). Moreover, coinfection mice exhibited much higher viral replication (Fig. 1F) and bacterial load (Fig. 1G), suggesting that coinfection severely impairs host resistance to viral and bacterial infections. However, HCPM or HCP treatment significantly decreased viral replication and bacterial load. Besides, we found that HCPM and HCP significantly inhibited the massive explosion of proinflammatory cytokines, including TNF-α (Fig. 1H), IL-6 (Fig. 1I), IFN-α (Fig. 1J), IFN-β (Fig. 1K), IFN-γ (Fig. 1L), and MPO (Fig. 1M) in the lungs. Taken together, our results indicate that HCPM and HCP without *in vitro* antiviral and *in vitro* antimicrobial effects alleviate coinfection-induced pneumonia.

3.2. *HCPM and HCP alleviate intestinal injury in viral-bacterial coinfection mice*

In coinfection mice, we observed not only severe lung lesions; but also small intestinal injury. H&E staining revealed that the control mice did not exhibit obvious histopathological changes (Fig. 2A). However, coinfection mice developed profound enteritis that most strongly manifested as disheveled and shortened villi, destroyed crypts, and inflammatory cell infiltration (Fig. 2A). The pathological lesions of the intestinal tract were markedly ameliorated by HCPM or HCP (Fig. 2A).

Intestinal goblet cells and their secreted mucous substances isolate the intestinal mucosal epithelium from the intestinal contents, which protects the mucosal epithelium. Our results indicated that HCPM and HCP promoted mucin secretion (blue) by goblet cells (Fig. 2B). Tight junctions (TJs) including ZO-1, Claudin-1, and Occludin between intestinal epithelial cells are important components of the intestinal epithelial barrier and inhibit the penetration of luminal antigens, environmental toxins, and bacteria, thus preventing potential focal enteropathy or systemic disease[55]. The immunofluorescence results indicated that coinfection decreased the expression of ZO-1 (Fig. 2C and F), Occludin (Fig. 2D and G), and Claudin-1 (Fig. 2E and H) in the small intestine, which were restored by HCPM or HCP treatment. In addition, treatment with HCPM or HCP effectively decreased the concentration of the proinflammatory cytokines IL-6 (Fig. 2I), IFN-γ (Fig. 2J), and MPO (Fig. 2K) in the small intestine. Taken together, the results indicate that HCPM and HCP ameliorate intestinal injury in coinfection mice.

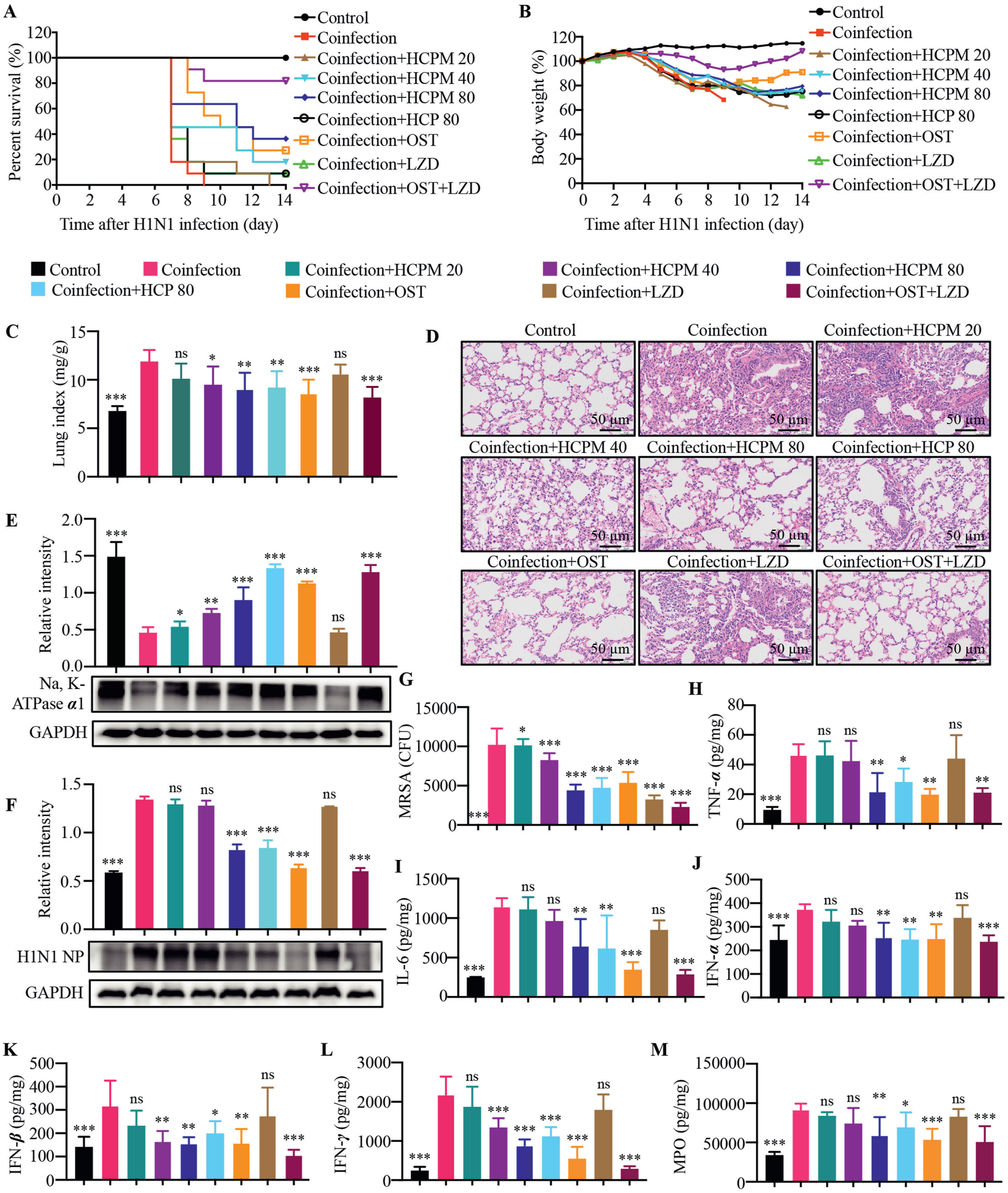

Figure 1 A homogeneous polysaccharide from *Houttuynia cordata* (HCPM) and crude polysaccharides from *Houttuynia cordata* (HCP) mitigate pneumonia severity in virus–bacterial coinfection mice. (A, B) C57BL/6 mice were infected intranasally with 0.2 LD_{50} influenza A virus (H1N1) and then infected 10^7 CFU methicillin-resistant *Staphylococcus aureus* (MRSA) three days later (11 mice in each group). C57BL/6 mice were treated with the indicated drugs once daily for seven days *via* gavage, beginning 2 h after viral infection. Survival rate (A) and body weight (B) were continuously monitored for 14 days. (C–N) C57BL/6 mice were infected intranasally with 0.2 LD_{50} H1N1 and then infected with 10^7 CFU MRSA 3 days later. Mice were treated with indicated drugs once daily for 5 days (6 mice in each group). (C) Lung index (the ratio of lung weight to body weight). (D) Histopathological injury and inflammatory infiltration of representative lung sections in each group. Scale bar = 50 μm. (E) Western blotting analysis of edema clearance-related proteins (Na,K-ATPase α1) in lung homogenates (n = 3). (F) The expression of viral nucleoprotein (NP) (n = 3). (G) Bacterial loads in mice lungs (n = 6). The concentration of the cytokines including TNF-α (H), IL-6 (I), IFN-α (J), IFN-β (K), IFN-γ (L), and MPO (M) in lungs were determined using ELISA (n = 5). Data are represented as mean ± SD and analyzed by one-way ANOVA followed by Dunnett's multiple comparisons test. P values < 0.05 were considered statistically significant, $^*P < 0.05$, $^{**}P < 0.01$, and $^{***}P < 0.001$ *vs.* coinfection; not significant (ns).

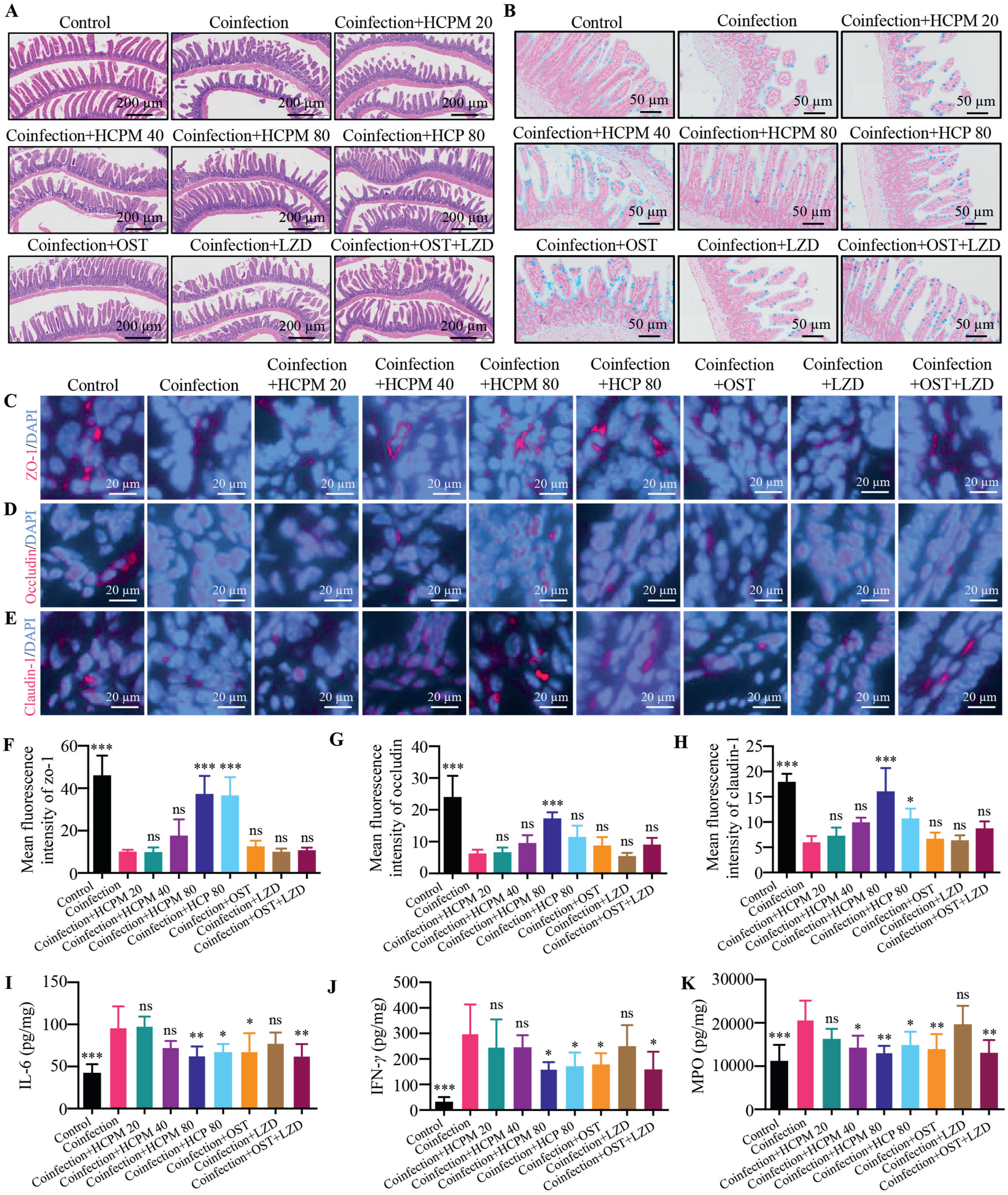

Figure 2 HCPM and HCP alleviate intestinal injury in viral–bacterial coinfection mice. C57BL/6 mice were infected intranasally with 0.2LD$_{50}$ H1N1 and then infected with 10^7 CFU MRSA three days later. Mice were treated with indicated drugs once daily for five days (6 mice in each group). (A) Morphological observation of intestinal epithelial integrity. Histopathological examination of small intestines through H&E staining ($n = 4$). Scale bar = 200 μm. (B) Mucin (blue) was detected by alcian blue & nuclear fast red staining kit ($n = 4$). Scale bar: 50 μm. (C–E) Immunofluorescent staining of TJ proteins including ZO-1 (C), Occludin (D), and Claudin-1 (E) in the small intestine. Images are representative of three individual experiments. Scale bar = 20 μm. (F–H) Mean fluorescence intensity of ZO-1 (F), Occludin (G), and Claudin-1 (H) ($n = 3$). (I–K) The concentration of IL-6 (I), IFN-γ (J), and MPO (K) in small intestine homogenates were determined using ELISA ($n = 5$). Data are represented as mean ± SD and analyzed by one-way ANOVA followed by Dunnett's multiple comparisons test. P values < 0.05 were considered statistically significant, $^*P < 0.05$, $^{**}P < 0.01$, and $^{***}P < 0.001$ *vs.* coinfection; not significant (ns).

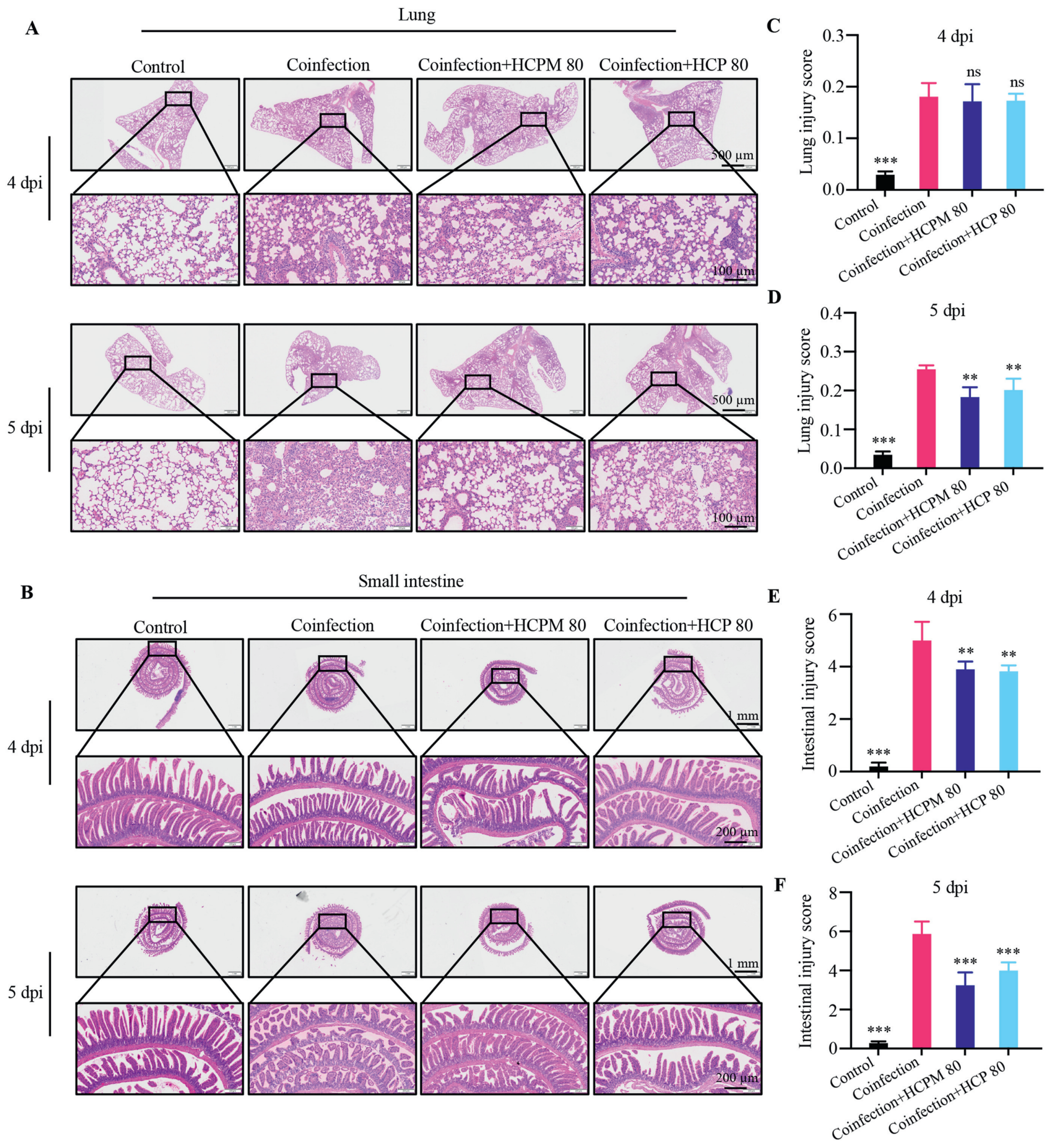

Figure 3 The therapeutic effect of HCPM and HCP on intestinal injury precedes lung injury in viral−bacterial coinfection mice. (A) Representative H&E images in the lungs on Day 4/Day 5 ($n = 4$). The overall picture, scale bar = 500 μm; local picture, scale bar = 100 μm. (B) Representative H&E images in the small intestines on Day 4/Day 5 ($n = 4$). The overall picture, scale bar = 1 mm; local picture, scale bar = 200 μm. (C−F) Histological score. Data are represented as mean ± SD and analyzed by one-way ANOVA followed by Dunnett's multiple comparisons test. P values < 0.05 were considered statistically significant, $^{**}P < 0.01$ and $^{***}P < 0.001$ *vs.* coinfection; not significant (ns).

3.3. *The therapeutic effect of HCPM and HCP on intestinal injury precedes lung injury in viral-bacterial coinfection mice*

Based on the above studies, we next focused on the dynamic effects of HCPM and HCP on the lung−gut axis. To achieve this objective, we observed the pathological changes in the lungs and small intestines of coinfection mice at 4 dpi and 5 dpi, respectively. As shown in Fig. 3A and B, coinfection caused a certain degree of lung−gut injury as early as 4 dpi. In addition, the severity of lung and small intestine lesions gradually increased with the progression of the coinfection. HCPM and HCP did not show an obvious impact on coinfection-induced lung injury at 4 dpi, but significantly alleviated lung pathology at 5 dpi (Fig. 3A, C, and D). Of note, HCPM and HCP treatment resulted in a significant alleviation in coinfection-induced small intestine injury at both 4 dpi and 5 dpi (Fig. 3E and F). These results indicate that the therapeutic effect of HCPM and HCP on intestinal injury precedes that of lung injury in coinfection mice, which may be attributed to its direct contact with the small intestine in prototype form. Thus, the results suggest that the small intestine may serve as the onset for HCPM and HCP to exert their effects.

3.4. *HCPM and HCP inhibit the overactivation of intestinal complement in viral-bacterial coinfection mice*

The focus of this study was HCPM. When the coinfection model establishment and drug effect were observed, no positive drug group was designed for further mechanistic studies or dynamic observation. Previous studies showed that HCPM exhibits potent anticomplement activity *in vitro* and *in vivo* and significantly attenuates H1N1-induced lung injury[35]. However, it is unclear whether HCPM and HCP can exert beneficial effects in coinfection mice through anticomplement activity. Excessive activation of the complement system occurs during viral or bacterial infection. C3a and C5a are anaphylatoxins produced during the activation of the complement system and participate in the activation of the NLRP3 inflammasome[12,18-21]. Compared with the control group, the coinfection group showed a significant increase of C3a and C5a in the small intestine as early as 4 dpi, with further increases observed at 5 dpi (Fig. 4). However, HCPM and HCP prominently inhibited the production of C3a and C5a in the small intestine as early as 4 dpi, and this effect persisted until 5 dpi (Fig. 4). Overall, the results indicate that HCPM and HCP inhibit intestinal complement activation in coinfection mice.

3.5. HCPM and HCP restrain the overactivation of intestinal NLRP3 inflammasome in viral-bacterial coinfection mice

We examined the activation of the intestinal NLRP3 inflammasome. To determine whether NLRP3 and cleaved-caspase-1 expression change in the gut of coinfection mice, we conducted an immunoblotting analysis of small intestine samples collected from coinfection mice and individuals without coinfection. A significant increase in NLRP3 (Fig. 5A, B, H and I) and cleaved-caspase-1 (Fig. 5A, C, H, and J) expression was observed in the

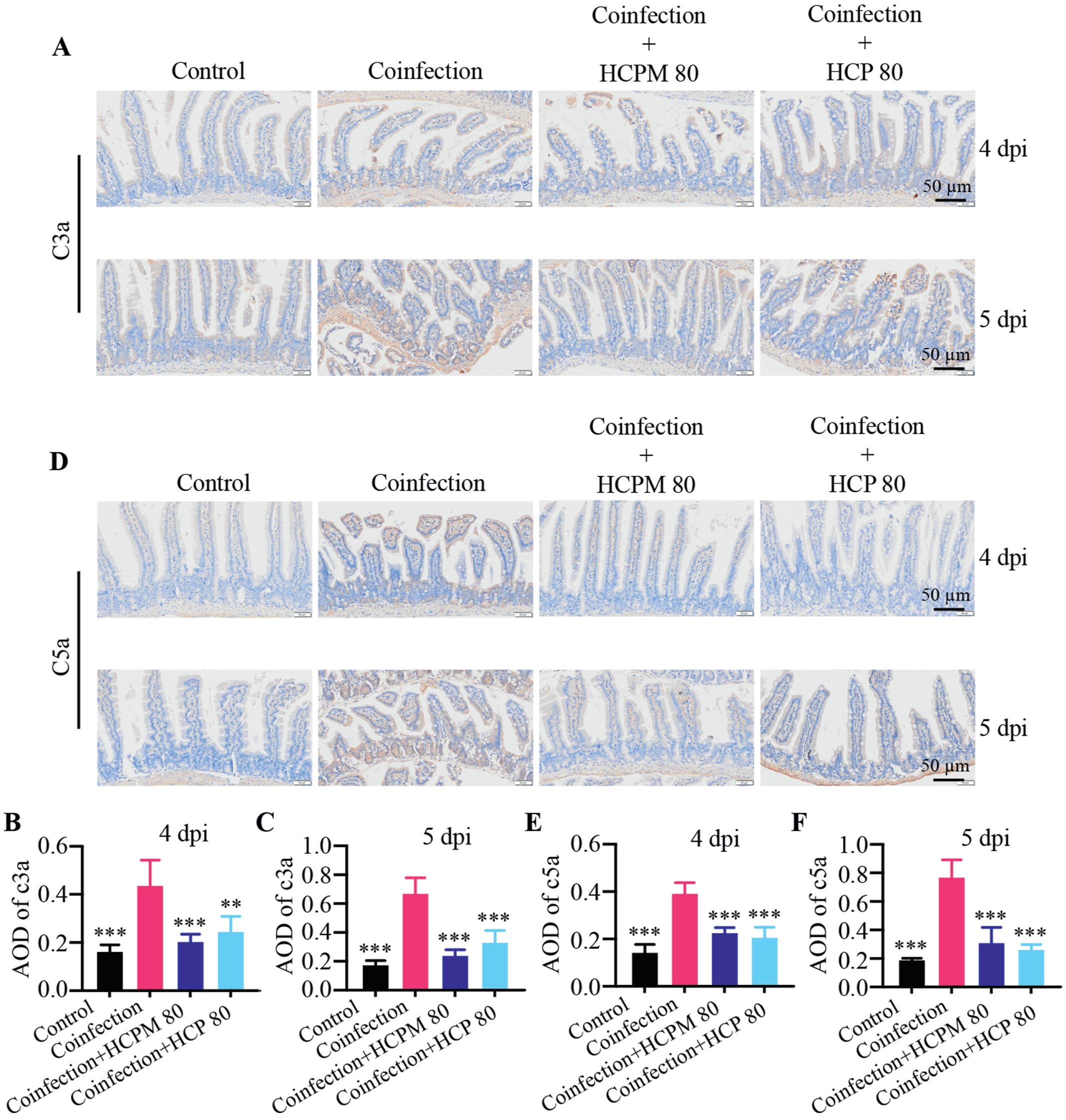

Figure 4 HCPM and HCP inhibit the overactivation of intestinal complement in viral−bacterial coinfection mice. C57BL/6 mice were infected intranasally with 0.2 LD_{50} H1N1 and then infected with 10^7 CFU MRSA three days later. Mice were treated with indicated drugs from Day 0 to Day 4 following H1N1 infection ($n = 6$). The small intestines were obtained from different groups on Day 4 and Day 5. (A) Representative images of immunohistochemical staining for C3a in small intestines ($n = 4$). (B, C) Quantitative analysis of the C3a-stained immunohistochemical images by ImageJ ($n = 4$). (D) Representative images of immunohistochemical staining for C5a in small intestines ($n = 4$). (E, F) Quantitative analysis of the C5a-stained immunohistochemical images by ImageJ ($n = 4$). Scale bar = 50 μm. Data are represented as mean ± SD and analyzed by one-way ANOVA followed by Dunnett's multiple comparisons test. P values < 0.05 were considered statistically significant, $^{**}P < 0.01$ and $^{***}P < 0.001$ *vs.* coinfection; not significant (ns).

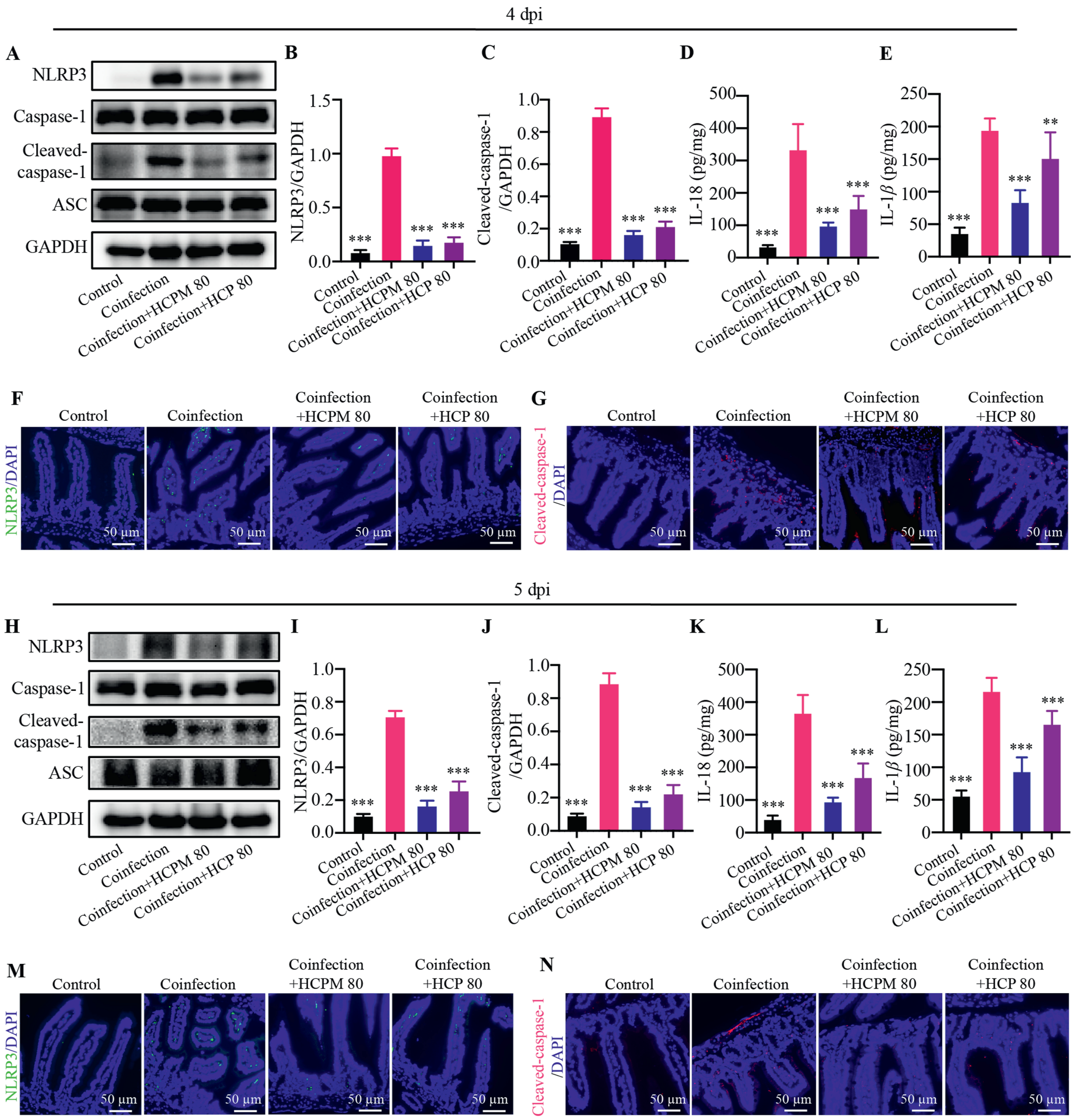

Figure 5 HCPM and HCP restrain the overactivation of intestinal NLR family pyrin domain-containing 3 (NLRP3) inflammasome in viral–bacterial coinfection mice. C57BL/6 mice were infected intranasally with 0.2 LD_{50} H1N1 and then infected with 10^7 CFU MRSA three days later. Mice were treated with indicated drugs for five days. The small intestines were obtained from different groups on Day 4 and Day 5. (A, H) The protein expression of NLRP3, cleaved-Caspase-1, Caspase-1, and ASC in small intestines was detected by Western blotting ($n = 3$). Densitometric analysis of NLRP3 (B, I), and cleaved-Caspase-1 (C, J) protein was performed. The contents of IL-18 and IL-1β in small intestinal tissue on Day 4 (D, E) and Day 5 (K, L) were detected by ELISA ($n = 6$). (F, M) Representative images of NLRP3 immunostaining in small intestine ($n = 4$). Scale bar = 50 μm. (G, N) Representative images of cleaved-Caspase-1 immunostaining in the small intestine ($n = 4$). Scale bar = 50 μm. Data are represented as mean ± SD and analyzed by one-way ANOVA followed by Dunnett's multiple comparisons test. P values < 0.05 were considered statistically significant, $^{**}P < 0.01$ and $^{***}P < 0.001$ *vs.* coinfection; not significant (ns).

small intestine obtained from coinfection subjects compared with the control subjects from 4 to 5 dpi.

HCPM and HCP treatment nearly eradicated NLRP3 and cleaved-caspase-1 protein expression (Fig. 5A–C and H–J). Next, we examined the fluorescence intensity of NLRP3 and cleaved-caspase-1. Similarly, the immunofluorescence showed that HCPM and HCP produced an inhibitory trend of NLRP3/cleaved-caspase-1 in the small intestine (Fig. 5F, G, M and N). IL-18 and IL-1β are key products of the NLRP3 inflammasome following activation. The results indicated that both HCPM and HCP significantly reduced the release of IL-18 (Fig. 5D and K) and IL-1β (Fig. 5E and L). This effect lasted from 4 to 5 dpi. Collectively, our results indicate that HCPM and HCP may regulate the intestinal NLRP3 inflammasome with inhibiting complement activation in coinfection mice.

3.6. The recovery effect of HCPM on Treg/Th17 cell imbalance may be related to its effect on NLRP3 inflammasome signaling in viral-bacterial coinfection mice

Multiple studies have shown that the NLRP3 inflammasome is involved in the imbalance of Treg/Th17 cells[23,29,30], which is a key immune mechanism in various respiratory diseases[26-28]. To further elucidate the role of intestinal NLRP3 inflammasome during coinfection, the NLRP3 inhibitor MCC950 was used to examine the Treg/Th17-mediated immune responses and pathological changes in the gut and lung. The inhibition of MCC950 on intestinal NLRP3 was confirmed by immunoblotting analysis (Supporting Information Fig. S5). Flow cytometry revealed that the coinfection group had a higher frequency of Th17 ($CD4^+IL\text{-}17A^+$) cells in LPs compared with that in the control group from 4 to 5 dpi, which was decreased by MCC950 treatment (Fig. 6A and B). The NLRP3 inhibitor restored the loss of Treg ($CD4^+Foxp3^+$) cells in $CD4^+$ T cells isolated from LPs (Fig. 6C and D). Further analysis revealed that the inhibition of intestinal NLRP3 contributed to the Treg/Th17 cells immune balance (Fig. 6E). In addition, MCC950 also reduced the frequency of Th17 cells in the lungs (Fig. 6F and G), increased the frequency of Treg cells (Fig. 6H and I), and promoting the balance of Treg/Th17 cells (Fig. 6J) in the lungs. More importantly, HCPM also promoted intestinal Treg/Th17 cell homeostasis and further improved pulmonary Treg/Th17 cell homeostasis. Moreover, treatment with MCC950 or HCPM ameliorated the intestinal (Supporting Information Fig. S6A) and pulmonary lesions (Fig. S6B). Thus, HCPM and MCC950 showed a similar effect on coinfection mice. Taken together, these results suggest that HCPM may improve Treg/Th17 cell imbalance in the gut−lung axis along with reducing the NLRP3 inflammasome activation, which contributes to improving the intestinal and pulmonary damage of coinfection mice.

3.7. HCPM and HCP regulate the balance of Treg and Th17 cells in the lung and intestinal mucosa during viral-bacterial coinfection

T cells in intestinal mucosa play an important role in regulating the homeostasis of the intestinal environment and affecting other mucosal sites[56]. Imbalanced Treg/Th17 cells in intestinal mucosa have been reported to be involved in the dysregulation of Treg/Th17 cells in the lungs in a model of viral pneumonia[26]. Therefore, we subsequently analyzed the changes of Th17/Treg cells in the lungs and small intestines. IL-17A and IL-10 were mainly produced by Th17 and Treg cells, respectively. Compared with the control group, coinfection resulted in a significant increase in IL-17A levels and a marked decrease in IL-10 levels in the lungs and small intestines, which were reversed following HCPM or HCP treatment (Supporting Information Fig. S7). However, IL-17A and IL-10 levels in the small intestines in the Oseltamivir, Linezolid, and Oseltamivir + Linezolid combination groups exhibited a trend of reversion, but there was no statistical significance. Further studies showed that the proportion of Treg/Th17 cells in LPs and lungs was significantly decreased in the coinfection group, suggesting an imbalance of Treg/Th17 cells in the local mucosa of the intestines and lungs, which is a key factor in coinfection-induced gut−lung injury. The administration of HCPM or HCP partially restored the Treg/Th17 cell balance in the LPs (Fig. 7C, D, and F) and lungs (Fig. 7A, B, and E). Oseltamivir or Oseltamivir + Linezolid combination partially reversed the imbalance of Treg/Th17 cells in the lungs, but not in the LPs. Moreover, Linezolid administration had no obvious effect on the imbalance of Treg/Th17 cells in the LPs and lungs. The spleen is the largest peripheral lymphatic organ in mammals and represents global immunity. Coinfection effectively decreased the proportion of Treg/Th17 cells in the spleen (Supporting Information Fig. S8), indicating a disruption of the immune balance in the spleen. However, HCPM or HCP did not affect the Treg/Th17 imbalance in the spleen (Fig. S8). Taken together, these results suggest that HCPM and HCP alleviate gut-lung injury in coinfection mice with modulating the ratio of Treg/Th17 cells in the local mucosa of the gut and lung.

3.8. HCPM and HCP restore the frequency of Treg and Th17 cells in the PP−MLN−lung axis in viral-bacterial coinfection mice

The mechanism of action of HCPM was further examined dynamically by measuring the percentages of Th17 and Treg cells in the lung and small intestine at different time points (Fig. 8A−F). After coinfection, the frequency of Th17 cells markedly increased in GALT (PPs and MLNs) and the lungs from 4 dpi. The frequency of Th17 in the PPs and MLNs, and the lungs remained at a high level on 5 dpi. HCPM or HCP treatment markedly reduced the frequency of Th17 cells in the PPs and MLNs from 4 to 5 dpi, and in the lungs on 5 dpi (Fig. 8A, C, and E). In contrast to Th17 cells, the percentage of Treg cells in the PPs, MLNs, and lungs was markedly decreased following coinfection (Fig. 8B, D, and F). HCPM or HCP treatment significantly upregulated the number of Treg cells in the PPs and MLNs from 4 to 5 dpi, and in the lungs on 5 dpi. Taken together, the results indicate that HCPM or HCP treatment restores the balance of Treg/Th17 cells first in the GALT followed by the lung (Supporting Information Fig. S9), which mitigates pneumonia resulting from viral-bacterial coinfection.

4. Discussion

Despite the clinical use of antiviral and antibacterial agents for patients with bacterial coinfections, the clinical efficacy of these drugs is not ideal because of the presence of drug resistance and mutated virus[46]. The advantages of TCM in preventing the progression of mild and moderate COVID-19 cases into severe and critical cases are notable and suitable for immediate application in epidemic prevention and treatment[57]. Of note, among the components of natural herbs, polysaccharides have emerged as important active constituents due to their prominent immunomodulation activity[58]. Natural polysaccharides, as macromolecular substances, are not easily absorbed into the blood through the gastrointestinal tract because of a lack of glycosidase for digestion in the human body. Most remain in their original form in the small intestine[59-61]. Macromolecular polysaccharides, such as HCP and HCPM, which are hard to be absorbed into the blood, have significant anti-complement activities and can attenuate complement-associated diseases[11,26,35,62]. However, it remains unclear whether HCPM and HCP have anti-complement activities and the potential immunomodulatory mechanisms in virus-bacterial coinfection mice. In this study, we established a coinfection murine model using virus (0.2 LD_{50} H1N1) and bacteria (10^7 CFU MRSA) (Fig. S1), and evaluated the therapeutic effects of HCPM and HCP on coinfection mice.

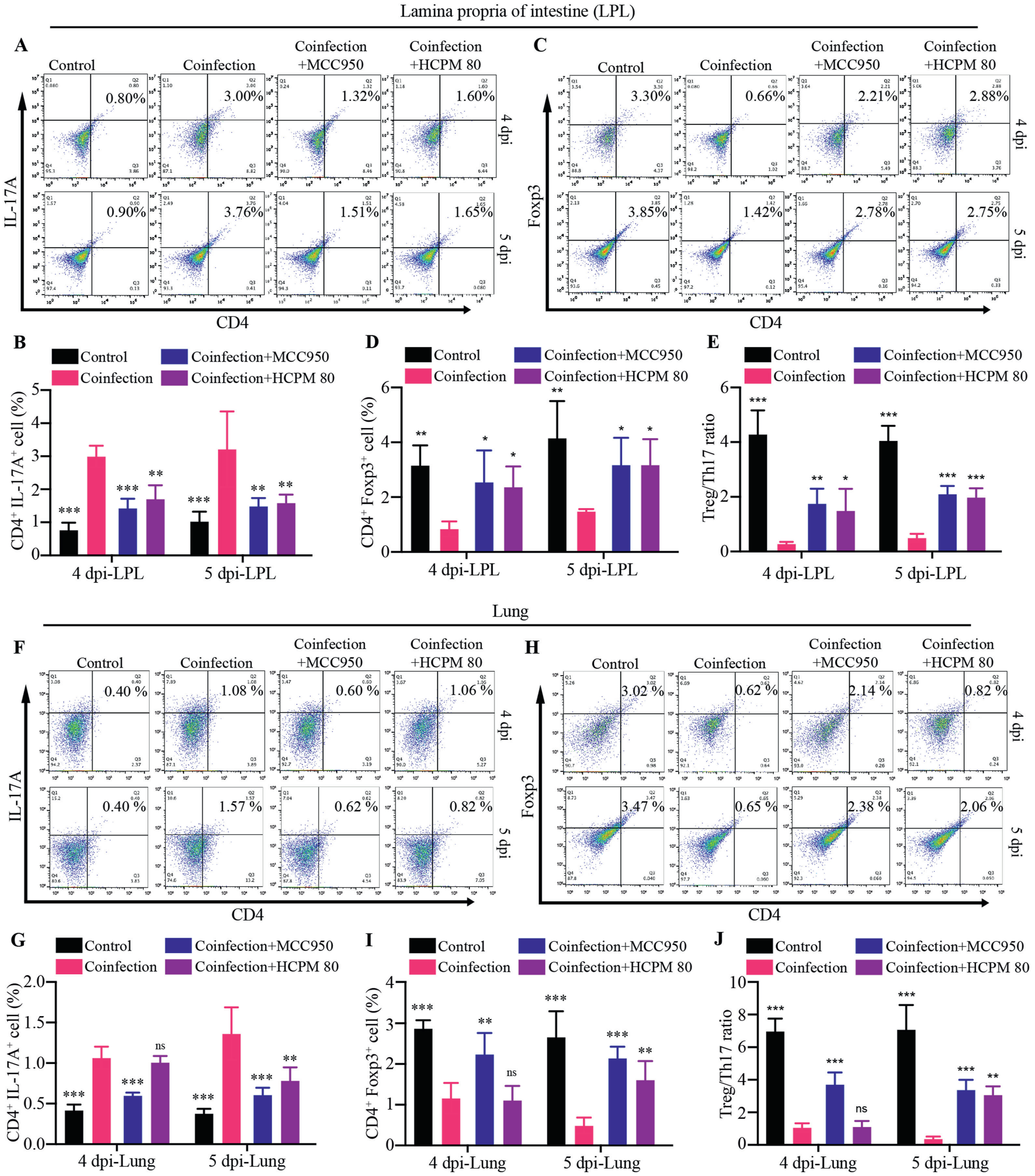

Figure 6 The recovery effect of HCPM on Treg/Th17 cell imbalance may be related to its effect on NLRP3 inflammasome signaling in viral−bacterial coinfection mice. C57BL/6 mice were infected intranasally with 0.2 LD_{50} H1N1 and then infected with 10^7 CFU MRSA three days later. Coinfection mice were treated with MCC950 (5 mg/kg, intraperitoneal injection) or HCPM (80 mg/kg, intragastric administration) from Day 0 to Day 4 following H1N1 infection. The intestinal lamina propria and lung were obtained from different groups on Day 4 and Day 5. The frequency of Th17 ($CD4^+IL\text{-}17A^+$) cells and Treg ($CD4^+Foxp3^+$) cells in intestinal lamina propria and lung were assayed using flow cytometry. (A, B) The changes of Th17 cells in intestinal lamina propria on Day 4 and Day 5 ($n = 4$). (C, D) The changes of Treg cells in intestinal lamina propria on Day 4 and Day 5 ($n = 4$). (E) The ratio of Treg/Th17 cells in intestinal lamina propria on Day 4 and Day 5 ($n = 4$). (F, G) The changes of Th17 cells in lungs on Day 4 and Day 5 ($n = 4$). (H, I) The changes of Treg cells in lungs on Day 4 and Day 5 ($n = 4$). (J) The ratio of Treg/Th17 cells in lungs on Day 4 and Day 5 ($n = 4$). Data are represented as mean ± SD and analyzed by one-way ANOVA followed by Dunnett's multiple comparisons test. P values < 0.05 were considered statistically significant, $^*P < 0.05$, $^{**}P < 0.01$, and $^{***}P < 0.001$ *vs.* coinfection; not significant (ns).

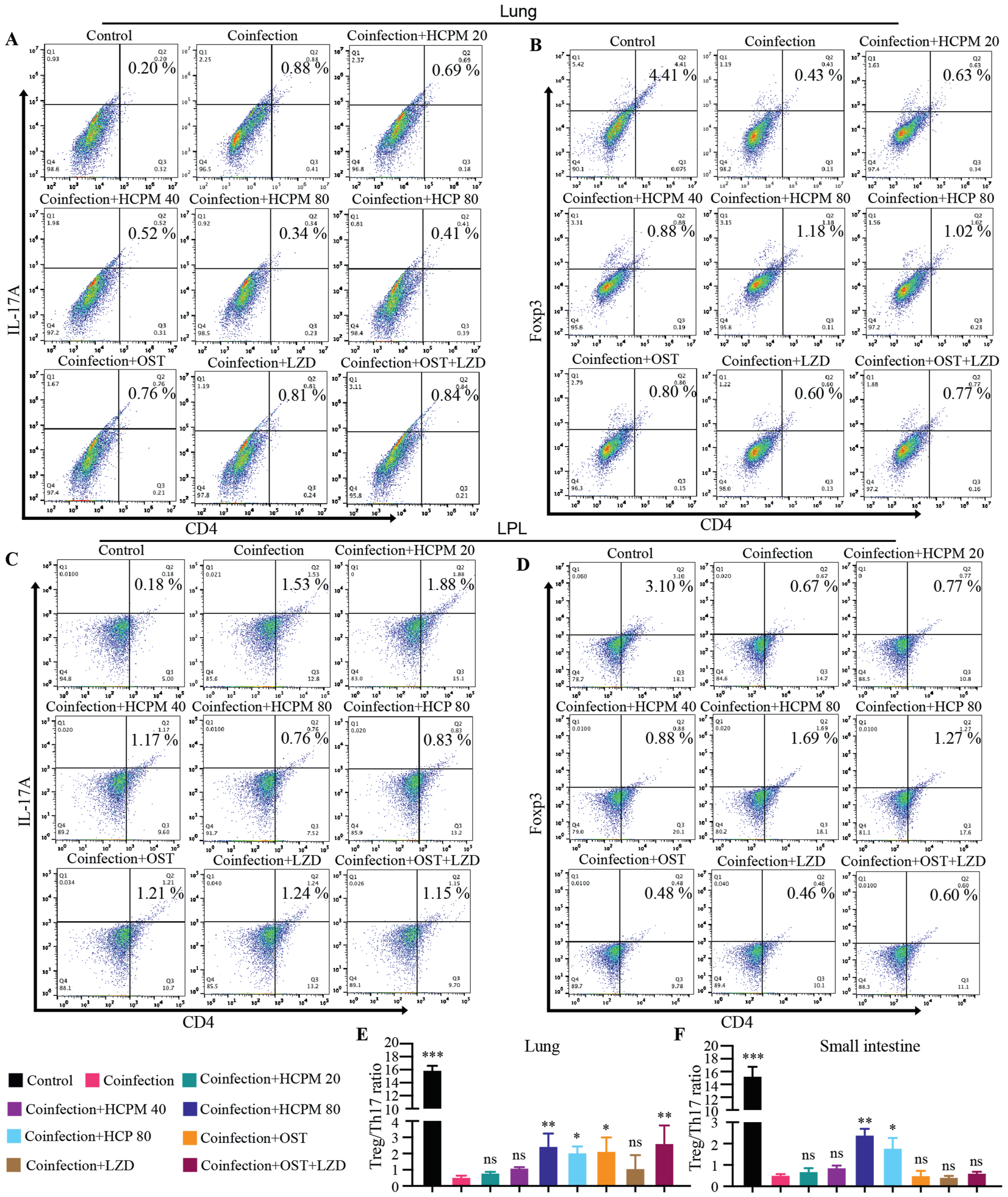

Figure 7 HCPM and HCP regulate the balance of Treg and Th17 cells in the lung and intestinal mucosa during viral—bacterial coinfection. C57BL/6 mice were infected intranasally with 0.2 LD_{50} H1N1 and then infected with 10^7 CFU MRSA three days later. Mice were treated with indicated drugs for five days. (A—D) The frequency of Th17 ($CD4^+IL\text{-}17A^+$) cells and Treg ($CD4^+Foxp3^+$) cells in the lungs and small intestines were assayed using flow cytometry ($n = 4$). (E) The ratio of Treg/Th17 cells in the lungs ($n = 4$). (F) The ratio of Treg/Th17 cells in small intestines ($n = 4$). Data are represented as mean ± SD and analyzed by one-way ANOVA followed by Dunnett's multiple comparisons test. P values < 0.05 were considered statistically significant, $^*P < 0.05$, $^{**}P < 0.01$, and $^{***}P < 0.001$ *vs.* coinfection; not significant (ns).

HCPM showed no *in vitro* antiviral (Fig. S3) and antimicrobial activity (Fig. S4). Our results indicated that HCPM alleviates lung injury in coinfection mice along with the inhibited proliferation of pulmonary viruses and bacteria, the low outbreak of proinflammatory factors, and reduced pulmonary edema (Fig. 1).

Lung injury impairs gas exchange, leading to systemic hypoxia, which in turn causes intestinal ischemia and hypoxia[34]. This further affects the integrity of the intestinal barrier[34]. Tight junction proteins (including ZO-1, Claudin-1, and Occludin) and mucin secreted by goblet cells are crucial for the integrity of the intestinal barrier, which is impaired by the changes in these factors[63]. A similar phenomenon of intestinal barrier impairment was observed in the H1N1—MRSA coinfection mice. However, HCPM or HCP treatment significantly reversed these damages and restored the intestinal barrier (Fig. 2A—H). Furthermore, HCPM or HCP significantly reduced the levels of intestinal inflammatory factors (IL-6, IFN-γ, and MPO) and mitigated intestinal mucosal damage (Fig. 2I—K).

Polysaccharides reach the small intestine primarily in their prototype form[63]. HCPM and HCP without *in vitro* antiviral and antibacterial effects could ameliorate coinfection-induced pneumonia, suggesting that their activity occurs through a unique

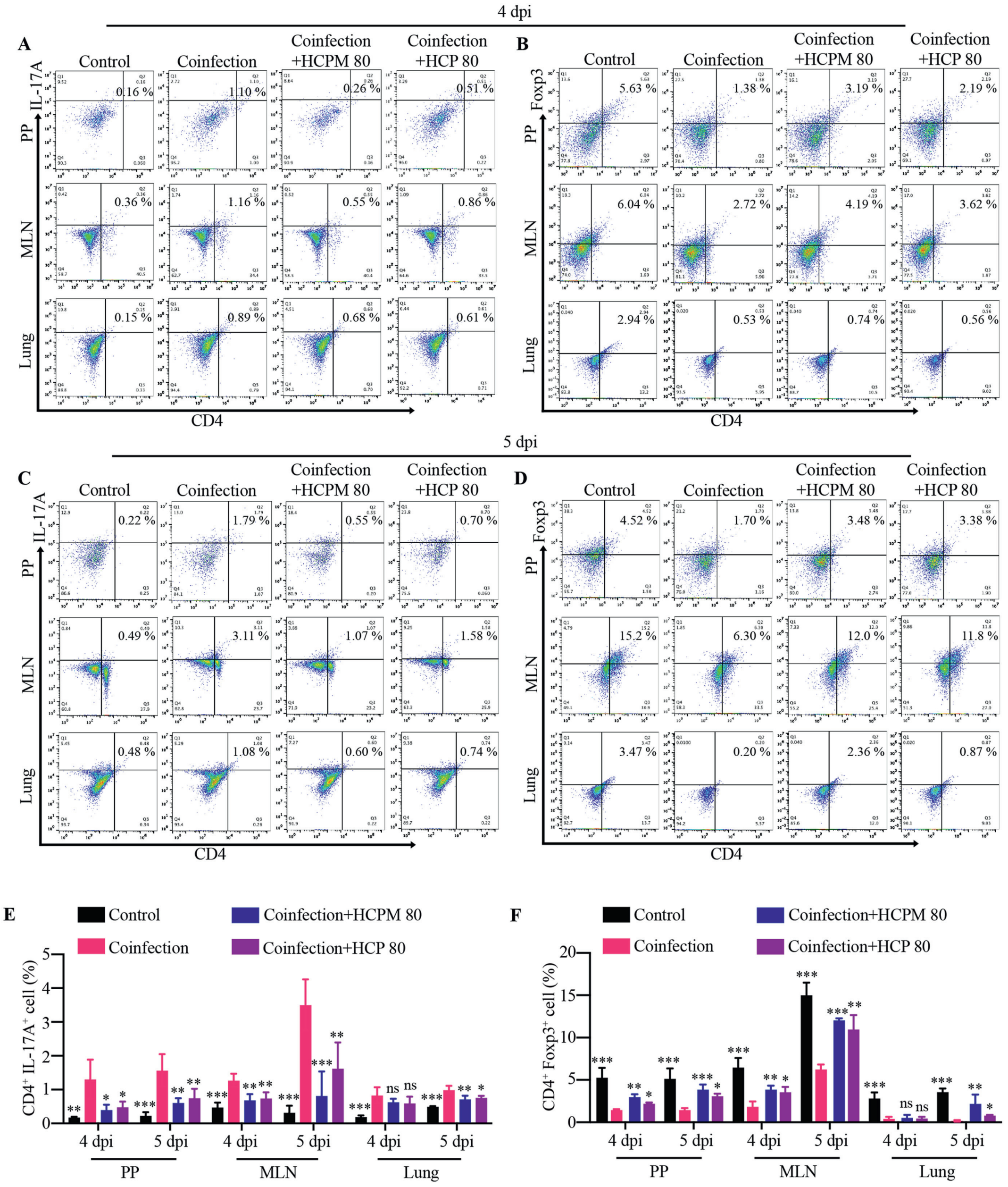

Figure 8 HCPM and HCP restore the frequency of Treg and Th17 cells in Peyer's patches (PPs)—mesenteric lymph nodes (MLNs)—lung axis in viral—bacterial coinfection mice. C57BL/6 mice were infected intranasally with 0.2 LD_{50} H1N1 and then infected with 10^7 CFU MRSA three days later. Mice were treated with indicated drugs for five days. The PPs, MLNs, and lungs were obtained from different groups on Day 4 and Day 5. (A—D) The frequency of Th17 ($CD4^+IL\text{-}17A^+$) cells and Treg ($CD4^+Foxp3^+$) cells in PPs, MLNs, and lungs were assayed using flow cytometry ($n = 4$). (E) The dynamic changes of Th17 cells in PPs, MLNs, and lungs ($n = 4$). (F) The dynamic changes of Treg cells in PPs, MLNs, and lungs ($n = 4$). Data are represented as mean ± SD and analyzed by one-way ANOVA followed by Dunnett's multiple comparisons test. P values < 0.05 were considered statistically significant, $^*P < 0.05$, $^{**}P < 0.01$, and $^{***}P < 0.001$ *vs.* coinfection; not significant (ns).

gut—lung pathway. Moreover, we observed that HCPM and HCP exhibited an earlier improvement in the small intestine compared with the lungs (Fig. 3), suggesting that the small intestine is most likely a direct target of HCPM and HCP. More experiments will be done in the future to further confirm the mechanism.

Excessive activation of the complement system occurs during viral or bacterial infections[35,64,65]. Complement fragments, C3a and C5a, are key anaphylatoxins. Clinical studies[16] have shown that anti-C5a antibodies or anti-C3 drugs (such as AMY-101) can improve the symptoms of patients with COVID-19, which gives us a new prospect of targeting the complement system in the treatment of major infectious lung diseases. Our study showed that inhibiting the hyperactivation of C3a and C5a may be beneficial to the coinfection mice (Fig. 4), highlighting the broad potential of complement system therapy.

C3a and C5a activate the NLRP3 inflammasome to amplify inflammation and exacerbate tissue damage[18-20]. Inhibiting the excessive activation of complement and NLRP3 inflammasome is helpful for the treatment of immunologic injury of intestinal tissue. Existing study[66] suggests that drugs that act as blockers of

NLRP3 inflammasome signaling may represent innovative strategies for the treatment of intestinal inflammation. In this study, we found that HCPM and HCP exerted a significant inhibitory effect on the excessive activation of the NLRP3 inflammasome (Fig. 5) located in the small intestine. This indicates that the inhibitory effects of HCPM or HCP on NLRP3 inflammasome might be associated with reduced gut complement activation. However, we just observed this phenomenon, and further investigation will be done to confirm the relationship between complement (C3a and C5a) and NLRP3 inflammasome.

The latest study[67] has shown that the gut complement system is regulated by the gut microbiota. Our previous study[68] showed that the beneficial effects of HCP on viral pneumonia were related to gut microbiota, suggesting that HCPM and HCP might also have a regulatory effect on intestinal flora in coinfection mice. It would be worthwhile to explore the biological links between polysaccharides and gut microbiota, complement and NLRP3 inflammasome in coinfection model.

A recent study[69] has revealed a novel communication pathway between the gut and lung, confirming that members of the gut microbiome tune pulmonary immunity through the gut-operated lung immune network (involving ILC2, T and B cells) to promote beneficial disease outcomes in response to pulmonary infections. The gut-lung axis is important for the immune response in respiratory diseases[36]. Interestingly, immune injury caused by coinfection not only occurs in the lung but also in the small intestine, which further supports the existence of the common mucosal immune system (CMIS). The CMIS protects against invasion of external pathogens in the respiratory and gastrointestinal tract and maintains host immune homeostasis[26]. T cells in the intestinal mucosa have an important role in regulating the homeostasis of the intestinal environment and affecting other mucosal sites[56]. Immune cells in GALT (PPs, MLNs), including T cells, migrate from the intestine to the lungs through the CMIS[70]. The spleen, which is the largest immune organ in the body, contains a substantial number of lymphocytes and macrophages, and serves as the central hub for both cellular and humoral immunity.

As crucial subsets of T cells, Treg cells are significantly reduced in viral- or bacterial-induced pulmonary diseases[26,27], whereas excessive activation of Th17 cells exacerbates lung inflammation[27,71]. Furthermore, an imbalance between Treg and Th17 cells has been observed in the majority of pulmonary inflammatory diseases[26-28]. More importantly, the imbalance in Treg/Th17 cells in GALT is involved in the dysregulation of Treg/Th17 cells in the lungs[26]. Related studies have revealed that an imbalance of Treg/Th17 cells is an indicator of COVID-19 severity[28]. Thus, modulating the balance between these cells, such as through mesenchymal stem cell therapy, may represent a potential treatment for COVID-19[72].

Of note, multiple studies have shown that the NLRP3 inflammasome is involved in the imbalance of Treg/Th17 cells[23,29,30], which is an important immune mechanism in various inflammatory diseases[26-28]. This potential mechanism has been rarely reported. A recent study[73] indicated that the NLRP3 inflammatory influences Th17 cell development and the conversion of Treg cells into Th17 cells through IL-1β, thus disrupting the Th17/Treg balance and exacerbating tissue inflammation. However, the specific mechanisms require further study. In coinfection mice, we found that direct inhibition of the NLRP3 inflammasome activity using MCC950 reversed intestinal Treg/Th17 cell imbalance and attenuated intestinal injury symptoms (Fig. 6A−E, Fig. S6A). Furthermore, we found that MCC950 restored the balance of Treg/Th17 cells in the lung and further alleviated pulmonary damage (Fig. 6F−J, Fig. S6B). HCPM showed a similar effect as MCC950. In this study, the NLRP3 inflammasome might be the potential target through which HCPM rebalanced Treg/Th17 cells to ameliorate coinfection-induced intestinal and pulmonary injury.

Our results indicate that coinfection causes an imbalance of Treg/Th17 cells in the lung and intestinal mucosa (Fig. 7, Fig. S2), and affects the balance of Treg/Th17 cells in the spleen (Fig. S8), which suggests an effect on CMIS and overall immunity. HCPM or HCP exerted therapeutic effects on coinfection mice, which rectified the Treg/Th17 imbalance in the lung and intestinal mucosa, but not in the spleen, which suggests that HCPM and HCP exhibit immunoregulation through the local mucosa. More importantly, the dynamic changes in the Treg/Th17 cells indicate that HCPM and HCP regulate the dysregulated Treg/Th17 cells in the small intestine prior to the lung (Fig. 8, Fig. S9). Our previous study[26] has confirmed that Treg/Th17 cells in the gut-associated lymphoid tissue (GALT) affect Treg/Th17 cells in the lung mucosa during the H1N1 virus infection. Furthermore, the therapeutic effect of HCP on H1N1 virus-induced pneumonia was confirmed to be dependent on the Treg and Th17 cells by gene knockout[26]. However, the possible mechanism by which the balance of Treg/Th17 cells in GALT affects the balance of Treg/Th17 cells in the lungs of H1N1−MRSA coinfection mice needs to be further investigated. Collectively, these results suggest that HCPM and HCP reduce lung injury in the coinfection mouse model by affecting the NLRP3 pathway and Treg/Th17 cell homeostasis in the gut−lung axis.

Currently, the clinical treatment for influenza virus−bacterial coinfection pneumonia primarily includes a combination of antiviral and antibacterial therapies. Representative antiviral drugs for influenza include Amantadine and Oseltamivir[74]. Amantadine has been widely used to treat influenza, but its further use has been limited by the rapid emergence of resistance[74]. Similar concerns have arisen for Oseltamivir[75]. In addition, the antigenic shift and drift of influenza viruses further increase the challenge of developing effective drugs[76]. Linezolid or Vancomycin has been used for MRSA infections. However, the emergence of low-susceptibility strains and nephrotoxicity has questioned the status of these therapies as first-line treatments[77,78]. In addition, the therapeutic window for antibiotic treatment is narrow and difficult to control. In this study, Oseltamivir or Linezolid alone had little effect on the survival rate of coinfection mice. However, Oseltamivir + Linezolid markedly improved the survival rate of coinfected mice (approximately 82%), which was related to their direct targeting effect on the pathogens. TCM has the characteristics of mild effect, multiple targets, low drug resistance, and low toxicity, especially prominent immunoregulation[79]. HCPM and HCP are natural components derived from *Houttuynia cordata* in TCM. As shown in Figs. S3 and S4, HCPM and HCP had no direct clearance effect on viruses or bacteria. However, they improved the survival rate of mice (36% and 10%, respectively) as well as coinfection pneumonia to a certain extent. It also suggests that HCPM and HCP play a role in the treatment of infectious lung diseases by regulating the host immune function without being restricted to the type of pathogen. Moreover, we speculated that the difference in efficacy between HCP and HCPM may be caused by the difference in composition, which needs to be further confirmed by subsequent experiments. Polysaccharides are essentially nontoxic and their safety profiles are significantly better compared with that of the combined administration of Oseltamivir and Linezolid[80]. We found that HCPM and HCP control the severity of coinfection through the regulation of some key inflammation-related targets (complement, NLRP3 inflammasome, Treg/Th17 cells), which provides insight for future drug development targeting related mechanisms. In the absence of targeted drugs for treating drug-resistant bacteria and/or mutated virus-infected lung diseases in the future, plant components may provide some help. *Houttuynia cordata* has been traditionally used to treat various respiratory tract infections in China. Our study confirmed that HCPM is a key component of *Houttuynia cordata* for the treatment of drug-resistant bacteria and virus coinfection.

Overall, our results indicate that polysaccharides from *Houttuynia cordata* exert therapeutic effects on pulmonary inflammatory diseases involving complex pathogen infection through multitarget effects. Nonetheless, there were some limitations to our study. The gut microbiota plays an important role in the intestinal immune response and respiratory system diseases[68]; however, several questions remain. How does the coinfection change the gut microbiota? Could HCPM or HCP interact with the gut microbiota to help ameliorate pneumonia caused by coinfection? These issues were not specifically addressed in the present study and warrant further investigation.

5. Conclusions

Unlike the antibiotics and antiviral drugs that directly against pathogens, anti-complement polysaccharides from *Houttuynia cordata* exert their therapeutic effects on coinfection mice by modulating the host immune response. Specifically, anti-complement polysaccharides from *Houttuynia cordata* may regulate the NLRP3 inflammasome and Treg/Th17 cell balance of the gut−lung axis, which contributes to improving coinfection-induced pneumonia. This study has enriched the connotation of the gut−lung axis, and expanded the potential medicinal values of *Houttuynia cordata* polysaccharides.

Acknowledgments

This study was supported by the National Natural Science Foundation of China (82030113).

Author contributions

Xinxing Li: Writing − original draft, Investigation, Data curation. Wenxin Ding: Investigation, Data curation. Yan Lu: Writing − review & editing, Project administration. Haiyan Zhu: Writing − review & editing. Weilian Bao: Writing − review & editing. Yang Liu: Formal analysis. Jiaren Lyu: Formal analysis. Lishuang Zhou: Formal analysis. Hong Li: Writing − review & editing. Jiyang Li: Writing − review & editing. Daofeng Chen: Writing − review & editing, Supervision, Project administration.

Conflicts of interest

The authors declare no conflicts of interest.

Appendix A. Supporting information

Supporting information to this article can be found online at https://doi.org/10.1016/j.apsb.2025.04.008.

References

1. Wu HY, Chang PH, Chen KY, Lin IF, Hsih WH, Tsai WL, et al. Coronavirus disease 2019 (COVID-19) associated bacterial coinfection: incidence, diagnosis and treatment. *J Microbiol Immunol Infect* 2022;**55**:985−92.
2. Iuliano AD, Roguski KM, Chang HH, Muscatello DJ, Palekar R, Tempia S, et al. Estimates of global seasonal influenza-associated respiratory mortality: a modelling study. *Lancet* 2018;**391**:1285−300.
3. Shah NS, Greenberg JA, McNulty MC, Gregg KS, Jt Riddell, Mangino JE, et al. Bacterial and viral co-infections complicating severe influenza: incidence and impact among 507 U.S. patients, 2013−14. *J Clin Virol* 2016;**80**:12−9.
4. Rawson TM, Moore LSP, Zhu N, Ranganathan N, Skolimowska K, Gilchrist M, et al. Bacterial and fungal coinfection in individuals with coronavirus: a rapid review to support COVID-19 antimicrobial prescribing. *Clin Infect Dis* 2020;**71**:2459−68.
5. Arabi YM, Al-Omari A, Mandourah Y, Al-Hameed F, Sindi AA, Alraddadi B, et al. Critically ill patients with the middle east respiratory syndrome: a multicenter retrospective cohort study. *Crit Care Med* 2017;**45**:1683−95.
6. Arabi YM, Deeb AM, Al-Hameed F, Mandourah Y, Almekhlafi GA, Sindi AA, et al. Macrolides in critically ill patients with Middle East respiratory syndrome. *Int J Infect Dis* 2019;**81**:184−90.
7. Verma AK, Bauer C, Yajjala VK, Bansal S, Sun K. Linezolid attenuates lethal lung damage during postinfluenza methicillin-resistant *Staphylococcus aureus* pneumonia. *Infect Immun* 2019;**87**:e00538-19.
8. Oliva J, Terrier O. Viral and bacterial co-infections in the lungs: dangerous liaisons. *Viruses* 2021;**13**:1725.
9. Feng Z, Ren X, Duren Z, Wang Y. Human genetic variants associated with COVID-19 severity are enriched in immune and epithelium regulatory networks. *Phenomics* 2022;**2**:389−403.
10. Lubbers R, van Essen MF, van Kooten C, Trouw LA. Production of complement components by cells of the immune system. *Clin Exp Immunol* 2017;**188**:183−94.
11. Lu Y, Jiang Y, Ling L, Zhang Y, Li H, Chen D. Beneficial effects of *Houttuynia cordata* polysaccharides on "two-hit" acute lung injury and endotoxic fever in rats associated with anti-complementary activities. *Acta Pharm Sin B* 2018;**8**:218−27.
12. Zhang Y, Han K, Du C, Li R, Liu J, Zeng H, et al. Carboxypeptidase B blocks *ex vivo* activation of the anaphylatoxin-neutrophil extracellular trap axis in neutrophils from COVID-19 patients. *Crit Care* 2021;**25**:51.
13. Morgan BP, Harris CL. Complement therapeutics; history and current progress. *Mol Immunol* 2003;**40**:159−70.
14. Mulligan MS, Schmid E, Beck-Schimmer B, Till GO, Friedl HP, Brauer RB, et al. Requirement and role of C5a in acute lung inflammatory injury in rats. *J Clin Investig* 1996;**98**:503−12.
15. Ember JA, Hugli TE. Complement factors and their receptors. *Immunopharmacology* 1997;**38**:3−15.
16. Risitano AM, Mastellos DC, Huber-Lang M, Yancopoulou D, Garlanda C, Ciceri F, et al. Complement as a target in COVID-19?. *Nat Rev Immunol* 2020;**20**:343−4.
17. Noris M, Remuzzi G. Overview of complement activation and regulation. *Semin Nephrol* 2013;**33**:479−92.
18. Kalbitz M, Fattahi F, Grailer JJ, Jajou L, Malan EA, Zetoune FS, et al. Complement-induced activation of the cardiac NLRP3 inflammasome in sepsis. *FASEB J* 2016;**30**:3997−4006.
19. Zhang T, Wu KY, Ma N, Wei LL, Garstka M, Zhou W, et al. The C5a/C5aR2 axis promotes renal inflammation and tissue damage. *JCI Insight* 2020;**5**:e134081.
20. Asgari E, Le Friec G, Yamamoto H, Perucha E, Sacks SS, Köhl J, et al. C3a modulates IL-1β secretion in human monocytes by regulating ATP efflux and subsequent NLRP3 inflammasome activation. *Blood* 2013;**122**:3473−81.
21. Friščić J, Böttcher M, Reinwald C, Bruns H, Wirth B, Popp SJ, et al. The complement system drives local inflammatory tissue priming by

metabolic reprogramming of synovial fibroblasts. *Immunity* 2021;**54**. 1002-21.e1010.

22. Kelley N, Jeltema D, Duan Y, He Y. The NLRP3 inflammasome: an overview of mechanisms of activation and regulation. *Int J Mol Sci* 2019;**20**:3328.
23. Chen L, Hou W, Liu F, Zhu R, Lv A, Quan W, et al. Blockade of NLRP3/Caspase-1/IL-1β regulated Th17/Treg immune imbalance and attenuated the neutrophilic airway inflammation in an ovalbumin-induced murine model of asthma. *J Immunol Res* 2022; **2022**:9444227.
24. Elinav E, Strowig T, Henao-Mejia J, Flavell RA. Regulation of the antimicrobial response by NLR proteins. *Immunity* 2011;**34**:665−79.
25. Willingham SB, Allen IC, Bergstralh DT, Brickey WJ, Huang MT, Taxman DJ, et al. NLRP3 (NALP3, Cryopyrin) facilitates *in vivo* caspase-1 activation, necrosis, and HMGB1 release *via* inflammasome-dependent and -independent pathways. *J Immunol* 2009;**183**:2008−15.
26. Shi CC, Zhu HY, Li H, Zeng DL, Shi XL, Zhang YY, et al. Regulating the balance of Th17/Treg cells in gut−lung axis contributed to the therapeutic effect of *Houttuynia cordata* polysaccharides on H1N1-induced acute lung injury. *Int J Biol Macromol* 2020;**158**:52−66.
27. Wen L, Shi L, Kong XL, Li KY, Li H, Jiang DX, et al. Gut microbiota protected against *Pseudomonas aeruginosa* pneumonia *via* restoring Treg/Th17 balance and metabolism. *Front Cell Infect Microbiol* 2022; **12**:856633.
28. Muyayalo KP, Huang DH, Zhao SJ, Xie T, Mor G, Liao AH. COVID-19 and Treg/Th17 imbalance: potential relationship to pregnancy outcomes. *Am J Reprod Immunol* 2020;**84**:e13304.
29. Pan Y, Wu Y, Liu Y, Wang P, Huang H, Jin J, et al. Long non-coding RNA ENSMUST00000197208 promotes a shift in the Th17/Treg ratio *via* the P2X7R−NLRP3 inflammasome axis in collagen-induced arthritis. *Immunol Res* 2024;**72**:347−60.
30. Zhang Q, Wang S, Ji S. Trifolirhizin regulates the balance of Th17/Treg cells and inflammation in the ulcerative colitis mice through inhibiting the TXNIP-mediated activation of NLRP3 inflammasome. *Clin Exp Pharmacol Physiol* 2022;**49**:787−96.
31. Li GZ, Chai OH, Lee MS, Han EH, Kim HT, Song CH. Inhibitory effects of *Houttuynia cordata* water extracts on anaphylactic reaction and mast cell activation. *Biol Pharm Bull* 2005;**28**:1864−8.
32. Chang JS, Chiang LC, Chen CC, Liu LT, Wang KC, Lin CC. Antileukemic activity of *Bidens pilosa* L. Var. minor (Blume) Sherff and *Houttuynia cordata* Thunb. *Am J Chin Med* 2001;**29**:303−12.
33. Lu HM, Liang YZ, Yi LZ, Wu XJ. Anti-inflammatory effect of *Houttuynia cordata* injection. *J Ethnopharmacol* 2006;**104**:245−9.
34. Zhu H, Lu X, Ling L, Li H, Ou Y, Shi X, et al. *Houttuynia cordata* polysaccharides ameliorate pneumonia severity and intestinal injury in mice with influenza virus infection. *J Ethnopharmacol* 2018;**218**: 90−9.
35. Zhou L, Jiao Y, Tang J, Zhao Z, Zhu H, Lu Y, et al. Ultrafiltration isolation, structure and effects on H1N1-induced acute lung injury of a heteropolysaccharide from *Houttuynia cordata*. *Int J Biol Macromol* 2022;**222**:2414−25.
36. Wang L, Cai Y, Garssen J, Henricks PAJ, Folkerts G, Braber S. The bidirectional gut−lung axis in chronic obstructive pulmonary disease. *Am J Respir Crit Care Med* 2023;**207**:1145−60.
37. Jia W, Li H, Zhao L, Nicholson JK. Gut microbiota: a potential new territory for drug targeting. *Nat Rev Drug Discov* 2008;**7**:123−9.
38. Rubinstein A. Natural polysaccharides as targeting tools of drugs to the human colon. *Drug Dev Res* 2010;**50**:435−9.
39. Reed LJ, Muench H. A simple method of estimating fifty per cent endpoints. *Am J Epidemiol* 1938;**27**:493−7.
40. Vimalanathan S, Schoop R, Suter A, Hudson J. Prevention of influenza virus induced bacterial superinfection by standardized *Echinacea purpurea, via* regulation of surface receptor expression in human bronchial epithelial cells. *Virus Res* 2017;**233**:51−9.
41. Li XX, Yuan R, Wang QQ, Han S, Liu Z, Xu Q, et al. Rotundic acid reduces LPS-induced acute lung injury *in vitro* and *in vivo* through regulating TLR4 dimer. *Phytother Res* 2021;**35**:4485−98.
42. Zhi HJ, Zhu HY, Zhang YY, Lu Y, Li H, Chen DF. *In vivo* effect of quantified flavonoids-enriched extract of *Scutellaria baicalensis* root on acute lung injury induced by influenza A virus. *Phytomedicine* 2019;**57**:105−16.
43. Esteban P, Redrado S, Comas L, Domingo MP, Millán-Lou MI, Seral C, et al. *In vitro* and *in vivo* antibacterial activity of gliotoxin alone and in combination with antibiotics against *Staphylococcus aureus*. *Toxins (Basel)* 2021;**13**:85.
44. Yi T, Ding W, Hao Y, Cen L, Li J, Shi X, et al. Neutrophil extracellular traps mediate severe lung injury induced by influenza A virus H1N1 in mice coinfected with *Staphylococcus aureus*. *Microb Pathog* 2022; **166**:105558.
45. Ling L, Ren A, Lu Y, Zhang Y, Zhu H, Tu P, et al. The synergistic effect and mechanisms of flavonoids and polysaccharides from *Houttuynia cordata* on H1N1-induced pneumonia in mice. *J Ethnopharmacol* 2023;**302**:115761.
46. Song J, Zhao J, Cai X, Qin S, Chen Z, Huang X, et al. Lianhuaqingwen capsule inhibits non-lethal doses of influenza virus-induced secondary *Staphylococcus aureus* infection in mice. *J Ethnopharmacol* 2022;**298**:115653.
47. Uyeki TM, Bernstein HH, Bradley JS, Englund JA, File TM, Fry AM, et al. Clinical Practice Guidelines by the Infectious Diseases Society of America: 2018 update on diagnosis, treatment, chemoprophylaxis, and institutional outbreak management of seasonal influenzaa. *Clin Infect Dis* 2019;**68**:895−902.
48. Lê VB, Schneider JG, Boergeling Y, Berri F, Ducatez M, Guerin JL, et al. Platelet activation and aggregation promote lung inflammation and influenza virus pathogenesis. *Am J Respir Crit Care Med* 2015; **191**:804−19.
49. Wang D, Deng B, Cheng L, Li J, Zhang J, Zhang X, et al. A novel and low-toxic peptide DR3penA alleviates pulmonary fibrosis by regulating the MAPK/miR-23b-5p/AQP5 signaling axis. *Acta Pharm Sin B* 2023;**13**:722−38.
50. Xu L, Yu Y, Sang R, Ge B, Wang M, Zhou H, et al. Inonotus obliquus polysaccharide protects against adverse pregnancy caused by *Toxoplasma gondii* infection through regulating Th17/Treg balance *via* TLR4/NF-κB pathway. *Int J Biol Macromol* 2020;**146**:832−40.
51. Means TK, Hayashi F, Smith KD, Aderem A, Luster AD. The Toll-like receptor 5 stimulus bacterial flagellin induces maturation and chemokine production in human dendritic cells. *J Immunol* 2003;**170**:5165−75.
52. Glaysher BR, Mabbott NA. Isolated lymphoid follicle maturation induces the development of follicular dendritic cells. *Immunology* 2007; **120**:336−44.
53. Xu M, Duan XY, Chen QY, Fan H, Hong ZC, Deng SJ, et al. Effect of compound sophorae decoction on dextran sodium sulfate (DSS)-induced colitis in mice by regulating Th17/Treg cell balance. *Biomed Pharmacother* 2019;**109**:2396−408.
54. Mairbäurl H, Wodopia R, Eckes S, Schulz S, Bärtsch P. Impairment of cation transport in A549 cells and rat alveolar epithelial cells by hypoxia. *Am J Physiol* 1997;**273**:L797−806.
55. Huang S, Wang X, Xie X, Su Y, Pan Z, Li Y, et al. Dahuang Mudan decoction repairs intestinal barrier in chronic colitic mice by regulating the function of ILC3. *J Ethnopharmacol* 2022;**299**:115652.
56. Metsälä J, Lundqvist A, Virta LJ, Kaila M, Gissler M, Virtanen SM. Prenatal and post-natal exposure to antibiotics and risk of asthma in childhood. *Clin Exp Allergy* 2015;**45**:137−45.
57. Huang K, Zhang P, Zhang Z, Youn JY, Wang C, Zhang H, et al. Traditional Chinese medicine (TCM) in the treatment of COVID-19 and other viral infections: efficacies and mechanisms. *Pharmacol Ther* 2021;**225**:107843.
58. Zhu N, Lv X, Wang Y, Li J, Liu Y, Lu W, et al. Comparison of immunoregulatory effects of polysaccharides from three natural herbs and cellular uptake in dendritic cells. *Int J Biol Macromol* 2016;**93**:940−51.
59. Jain A, Gupta Y, Jain SK. Perspectives of biodegradable natural polysaccharides for site-specific drug delivery to the colon. *J Pharm Pharmaceut Sci* 2007;**10**:86−128.
60. Li L, Yao H, Li X, Zhang Q, Wu X, Wong T, et al. Destiny of *Dendrobium officinale* polysaccharide after oral administration:

indigestible and nonabsorbing, ends in modulating gut microbiota. *J Agric Food Chem* 2019;**67**:5968−77.

61. Xiong Q, HaojieLi ShijieChen, YaoZhao YonglinJing, YiYuan JunLai. Xiaoping. Perspective: aggregation-induced emission as an emerging strategy for exploring pharmacokinetics of oral polysaccharides. *J Carbohydr Chem* 2018;**37**:61−8.
62. Xu YY, Zhang YY, Ou YY, Lu XX, Pan LY, Li H, et al. *Houttuyniacordata* Thunb. polysaccharides ameliorates lipopolysaccharide-induced acute lung injury in mice. *J Ethnopharmacol* 2015;**173**: 81−90.
63. Chen MY, Li H, Lu XX, Ling LJ, Weng HB, Sun W, et al. *Houttuynia cordata* polysaccharide alleviated intestinal injury and modulated intestinal microbiota in H1N1 virus infected mice. *Chin J Nat Med* 2019;**17**:187−97.
64. Zhang J, Huo J, Zhao Z, Lu Y, Hong Z, Li H, et al. An anticomplement homogeneous polysaccharide from *Hedyotis diffusa* attenuates lipopolysaccharide-induced acute lung injury and inhibits neutrophil extracellular trap formation. *Phytomedicine* 2022;**107**:154453.
65. Gil E, Noursadeghi M, Brown JS. *Streptococcus pneumoniae* interactions with the complement system. *Front Cell Infect Microbiol* 2022;**12**:929483.
66. Pellegrini C, Fornai M, Colucci R, Benvenuti L, D'Antongiovanni V, Natale G, et al. A comparative study on the efficacy of NLRP3 inflammasome signaling inhibitors in a pre-clinical model of bowel inflammation. *Front Pharmacol* 2018;**9**:1405.
67. Wu M, Zheng W, Song X, Bao B, Wang Y, Ramanan D, et al. Gut complement induced by the microbiota combats pathogens and spares commensals. *Cell* 2024;**187**:897−913.e818.
68. Shi C, Zhou L, Li H, Shi X, Zhang Y, Lu Y, et al. Intestinal microbiota metabolizing *Houttuynia cordata* polysaccharides in H1N1 induced pneumonia mice contributed to Th17/Treg rebalance in gut−lung axis. *Int J Biol Macromol* 2022;**221**:288−302.
69. Burrows K, Ngai L, Chiaranunt P, Watt J, Popple S, Forde B, et al. A gut commensal protozoan determines respiratory disease outcomes by shaping pulmonary immunity. *Cell* 2025;**188**. 316-30.e12.
70. Mestecky J. Saliva as a manifestation of the common mucosal immune system. *Ann N Y Acad Sci* 1993;**694**:184−94.
71. Bystrom J, Al-Adhoubi N, Al-Bogami M, Jawad AS, Mageed RA. Th17 lymphocytes in respiratory syncytial virus infection. *Viruses* 2013;**5**:777−91.
72. Motallebnezhad M, Hazrati A, Esmaeili Gouvarchin Ghaleh H, Jonaidi-Jafari N, Abbaspour-Aghdam S, Malekpour K, et al. Exosomes from adipose tissue-derived mesenchymal stem cells induce regulatory T cells in COVID-19 patients. *Iran J Allergy Asthma Immunol* 2023; **22**:233−44.
73. Liu X, Chen J, Yue S, Zhang C, Song J, Liang H, et al. NLRP3-mediated IL-1β in regulating the imbalance between Th17 and Treg in experimental autoimmune prostatitis. *Sci Rep* 2024;**14**:18829.
74. Xu J, Yu J, Yang L, Zhou F, Li H, Cao B. Influenza virus in community-acquired pneumonia: current understanding and knowledge gaps. *Semin Respir Crit Care Med* 2020;**41**:555−67.
75. Behillil S, May F, Fourati S, Luyt CE, Chicheportiche T, Sonneville R, et al. Oseltamivir resistance in severe influenza A(H1N1)pdm09 pneumonia and acute respiratory distress syndrome: a French multicenter observational cohort study. *Clin Infect Dis* 2020;**71**:1089−91.
76. Kumari R, Sharma SD, Kumar A, Ende Z, Mishina M, Wang Y, et al. Antiviral approaches against influenza virus. *Clin Microbiol Rev* 2023; **36**:e0004022.
77. Rodvold KA, McConeghy KW. Methicillin-resistant *Staphylococcus aureus* therapy: past, present, and future. *Clin Infect Dis* 2014; **58**(Suppl 1):S20−7.
78. Jia L, Zhao J, Yang C, Liang Y, Long P, Liu X, et al. Severe pneumonia caused by coinfection with influenza virus followed by methicillin-resistant *Staphylococcus aureus* induces higher mortality in mice. *Front Immunol* 2018;**9**:3189.
79. An X, Zhang Y, Duan L, Jin D, Zhao S, Zhou R, et al. The direct evidence and mechanism of traditional Chinese medicine treatment of COVID-19. *Biomed Pharmacother* 2021;**137**:111267.
80. Shi R, Dan B, Lü L. Bioactive effects advances of natural polysaccharides. *J Future Foods* 2023;**3**:234−9.